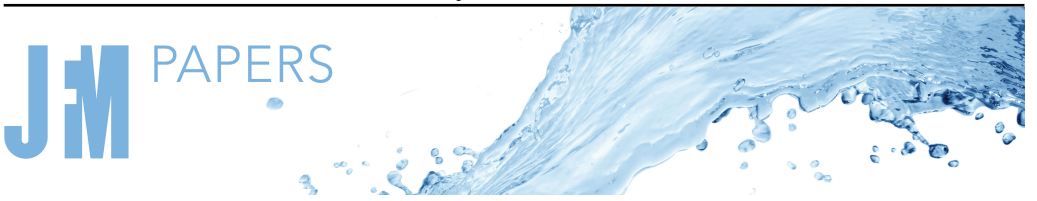
J. Fluid Mech. (2026), *vol.* 1045, A4, doi:10.1017/jfm.2026.12121



Wave scattering by a sloping beach of an arbitrary angle. Revisited: regular solution

Gennady Mishuris[1], **Michael H. Meylan**[2] **and Efim N. Pelinovsky**[3,4]

[1]Department of Mathematics, Aberystwyth University, Aberystwyth, Wales SY233BZ, UK

[2]School of Computer and Information Sciences, University of Newcastle, Newcastle, NSW 2300, Australia

[3]A.V. Gaponov-Grekhov Institute of Applied Physics, 46 Uljanov Street, Nizhny Novgorod 603950, Russia

[4]National Research University – Higher School of Economics (HSE), 25/12 Bolshaya Pecherskaya street, Nizhny Novgorod 603155, Russia

Corresponding author: Gennady Mishuris, ggm@aber.ac.uk

(Received 28 June 2025 UTC; revised 23 March 2026 UTC; accepted 3 August 2026 UTC)

In this paper, we revisit the classic problem of a wave field on a sloping beach of an arbitrary angle and propose a general approach that allows the computation of regular solutions of the problem regardless of the angle. We use the Mellin-transform technique, reducing the problem to singular integral equations with fixed-point singularities of a special kind. Exact formulas are provided for the reflection coefficient, phase shift and wave surge at the shoreline. We demonstrate the efficiency of the proposed approach in the frequency domain and use these results to compute time-dependent solutions. We compare our results with those known from the literature.

Key words: wave scattering, mathematical foundations

1. Introduction

The problem of wave run-up on the shore is of clear practical significance, for example, coastal flooding can have catastrophic consequences for both populations and infrastructure (Dean & Dalrymple 1991). Furthermore, exploitation of various coastal protection engineering devices and energy generating plants requires careful analysis of the interaction between waves and constructions (Rodriguez-Delgado *et al.* 2019; Singhvi *et al.* 2022). Finally, the interaction between water waves and sea ice cover plays one of the crucial roles in terms of environmental impacts (Bennetts *et al.* 2022). Due to the importance of such problems, numerical methods for solving hydrodynamic equations

© The Author(s), 2026. Published by Cambridge University Press. This is an Open Access article, distributed under the terms of the Creative Commons Attribution licence (https://creativecommons.org/licenses/by/4.0/), which permits unrestricted re-use, distribution and reproduction, provided the original article is properly cited.

https://doi.org/10.1017/jfm.2026.12121 Published online by Cambridge University Press

(such as the Euler and Navier–Stokes equations) are actively applied, accounting for the properties of the underlying surface and wave breaking. The literature on this topic is vast; we will refer only to Temam (2024).

Our focus is on analytical approaches to studying wave run-up. From a theoretical perspective, even in an idealised formulation (impermeable bottom, perfect fluid), this problem involves a nonlinear boundary value problem with an unknown moving boundary, presenting clear challenges for resolution. Significant progress has been achieved within the framework of the one-dimensional nonlinear shallow-water theory, where exact solutions for waves over a slope of constant inclination have been obtained (see Didenkulova 2009).

A pioneering work in this area is the paper by Carrier & Greenspan (1958), where the application of Legendre transformations allowed the nonlinear equations to be reduced to a linear wave equation. Physical variables (e.g. displacement of the water level, flow velocity, time and position) were determined by simple relationships derived from the solutions to this wave equation. This method, known as the Carrier–Greenspan transformation, has since been widely used in tsunami studies to estimate wave heights on the shore (e.g. Spielvogel 1976; Synolakis 1987; Pelinovsky & Mazova 1992; Kânoğlu & Synolakis 2006; Dobrokhotov *et al.* 2013).

Moreover, this approach has been generalised to inclined channels of arbitrary cross-sections in Pelinovsky & Mazova (1992) and Rybkin (2019). A key property of the Carrier–Greenspan transformation is its demonstration that linear theory can be used to evaluate critical wave characteristics – such as maximum heights and flow velocities on the shoreline – that hold significant practical value. This means that solving the linear problem for waves over a sloped bed with reflective boundary conditions provides displacements at the shoreline, which directly correspond to the extreme values of wave run-up heights in nonlinear shallow-water theory. Furthermore, criteria for initial wave breaking in nonlinear theory, such as gradient catastrophe, can also be expressed through wave field characteristics within the linear framework (Pelinovsky & Mazova 1992). Subsequently, such solutions have been applied to spatial Cauchy–Poisson problems and wave generation due to seabed displacement (Haugen & Tyvand 2003).

This finding supports the idea that linear solutions might be applicable in more general settings. The problem of linear monochromatic waves on an inclined shore is a classical problem analysed by Lewy (1946), Stoker (1947), Friedrichs (1948), Friedrichs & Lewy (1948), Isaacson (1950), Peters (1950) and Brillouet (1957) by means of complex analysis and discussed in foundational texts (e.g. Sretensky (1977), Stoker (2019), with closed-form solutions available for specific slope angles (e.g. $\pi/(2m)$, where m is a natural number). These solutions include singular ones on the shoreline, associated with wave breaking discussed in Sretensky (1977).

Ehrenmark has developed a substantial body of work on wave scattering on a sloping beach. In a series of papers, solutions were constructed in a closed form using Mellin-transform techniques. They were represented in terms of oscillatory integrals that were evaluated numerically. These works provide an important analytical description of the problem and include detailed investigations of the associated integral representations and numerical procedures for their evaluation. In particular, he has shown that his solutions are valid for every slope angle between 0 and $\pi/2$, although the limitations of computational power at that time meant that only discrete angles were computed in Ehrenmark (1987, 1989). Subsequently, these solutions were cited and used as first-order approximations in viscous boundary layer problems (see Ehrenmark 1991, 1994). In later papers (e.g. Ehrenmark 2006), the problem was extended to oblique wave incidence, using the inverse Kontorovich–Lebedev transform. This work also includes a discussion

https://doi.org/10.1017/jfm.2026.12121 Published online by Cambridge University Press

of another computational scheme, which employs the W-transform for the inner integrals, and is also applicable in the two-dimensional case. Other examples of successful use of the Mellin transform are analysis of the reflection of gravity waves by a beach with a porous bed in Body & Ehrenmark (1998) and the scattering of water waves by a floating elastic plate above a plane incline in Ehrenmark (2003, 2009) and Ehrenmark & Porter (2012). Finally, the Green function for the linear water wave problem was built and an algorithm was constructed for its accurate computation in the case $0 < \alpha < \pi/2$ in Ehrenmark (2009, 2011). Note that even though Ehrenmark mainly used his solution in the regions with an angle less than $\pi/2$, he underlined that it is also valid for the entire range of the slopes ($0 < \alpha \leqslant \pi$) and demonstrated this for the dock problem ($\alpha = \pi$) in Ehrenmark (2009) deriving an alternative representation for the solution to that of Friedrichs & Lewy (1948). It should be mentioned that a rigorous mathematical analysis of the linearised gravitational water wave problems in various domains those are: solvability (existence and uniqueness) and regularity of the solutions in appropriate functional spaces were provided in Shinbrot (1967), Ton (1987) and Kuznetsov *et al.* (2002)

Regardless of the method used to solve the linearised gravitational water wave problems mentioned above, they are all finally transformed to similar functional difference equations. Those, in turn, appear in classical problems defining many special functions (see, for example, Lawrie & King 1994) and also have arisen in fluid mechanics in Maliuzhinets (1958), and in fracture mechanics, for example, in Koiter (1955), Atkinson (1977) and Mishuris (1995*a*, 2001). Some of the equations corresponding to the linearised water wave theory on the sloping beach have been solved in terms of series, while the other have been solved by transforming the problem into singular integral equations (e.g. the dock problem, which is the limiting case of angle $\alpha = \pi$, by Chakrabarti *et al.* 2005).

However, existing solutions to this classical problem are often presented in disparate forms, and as a result, important insights developed within one framework are not always fully captured or utilised in others. Moreover, some of these approaches yield solutions that are either impractical for application or excessively technical, limiting their accessibility and reproducibility for a broader audience. These considerations motivate a renewed examination of the problem from an alternative analytical perspective that allows efficient practical implementation.

In this paper we follow Ehrenmark and use the Mellin integral transform method. The objective of this paper is not to reproduce previous results but to revisit the classical sloping beach problem from a distinct analytical perspective. We reformulate the problem for the regular water wave by reducing it to a non-classical singular integral equation of the third kind

$$f(x)p(x) + \mathcal{N}[p](x) = h_1(x) + dh_2(x), \quad 0 < x < \infty, \tag{1.1}$$

where $\mathcal{N}$ is a linear integral operator with fixed-point singularities defined in (2.69), the multiplier, $f(x) = 1 - x$, degenerates at point $x = 1$, $h_j(x)$ are known functions, and both a constant d and a function $p(x)$ are to be found from the condition $|p(1)| < \infty$.

Our approach is different from that used by Ehrenmark and produces a unified procedure to construct the solution and provides a convenient framework for numerical implementation, allowing high efficiency for an arbitrary slope angle in the full range $0 < \alpha \leqslant \pi$. Within this framework, we show the solvability of the integral equation (Statement 1) and demonstrate the efficacy of the resulting computational approach. Interestingly, in this approach, the reflection coefficient is computed from a necessary and sufficient condition for the solvability of the integral equation (the values of the constant d and the reflection coefficient R are related by a simple formula). We evaluate the structure of the regular solution (see (2.88)) following from this approach and confirm that all

https://doi.org/10.1017/jfm.2026.12121 Published online by Cambridge University Press

known relationship between the reflection coefficient, the phase shift, and the run-up are consistent with the known results discussed in classic papers by Stoker, Lewy, Friedrichs and Ehrenmark (Statements 2,3). In particular, the run-up computed as a functional on the solution of the integral equation (compare (2.92) and (2.93)). Our approach allows us to obtain a new exact relationship between the wave run-up and its inclination at the beach edge (Statement 4). This simple relationship, which, to the best of our knowledge, has not been derived previously, is important for implementation of various breaking criterion. All of these results are detailed in §§ 2 and 3.

To further validate the solutions obtained, in this paper we also consider a direct numerical technique based on the boundary element method (BEM). We use the solutions obtained in the frequency domain to compute the time-domain solution with arbitrary initial condition.

We note that the propagation of unsteady waves above a sloping beach was probably first studied in Keldysh (1937) within the framework of a linear dispersion model, where a solution of the three-dimensional problem was proposed for a very special angle $\alpha = \pi/4$. The two-dimensional problem was studied in Rumyantsev (1960), where asymptotic solutions were found for certain angles of α. Griffel & Morris (1977) exploited the scaling with respect to the wavenumber to provide a solution to the problem of waves forced by changing surface pressure. Later, Dorfman (1984) obtained solutions for the two- and three-dimensional problems of unsteady waves above an inclined floor, using the Laplace and Mellin transforms and incorporating classic results from Stoker (2019) for angles $\alpha = \pi/(2m)$.

The solution method we used is based on the transform given for a beach with constant slope by Ehrenmark & Body (2001), which is a special case of the general result given in Meylan (2009). We note that this formula (see (4.2)), for specific beach angles, appeared in Dorfman (1984) in Russian. We show that the integrals in the time-domain solution can be effectively approximated as a product of matrices that generalised the diagonalisation of self-adjoint matrices, based on recent results from Wilks *et al.* (2024, 2025).

We emphasise that the new approach, proposed in the paper to tackle the classic problem of wave scattering by a sloping beach, gives researchers additional flexibility in using different tools (those classical ones based on the complex analysis and attributed to Lewy, Friedrichs, Stoker and others (see Sretensky 1977; Stoker 2019), Ehrenmark's approach mentioned above in the introduction that used a specific closed-form solution representation obtained by Mellin transform that requires a delicate treatment, our approach, or a direct numerical simulation using a BEM). In short, each approach has its own advantages and disadvantages.

2. Wave scattering by a sloping beach

2.1. *Problem formulation*

We consider a classical problem for linearised potential flow (see Stoker 2019) describing the wave field on a beach with constant slope with angle α between the surface of the free water and the beach (bottom of the ocean). In the fluid domain Ω (see figure 1), given by

$$\Omega = \{(r, \theta): \quad 0 < r < \infty, \quad \pi < \theta < \theta_0 = \pi + \alpha \leqslant 2\pi\}, \tag{2.1}$$

the velocity potential $\phi(r, z)$ satisfies the Laplace equation

$$\Delta\phi = 0. \tag{2.2}$$

https://doi.org/10.1017/jfm.2026.12121 Published online by Cambridge University Press

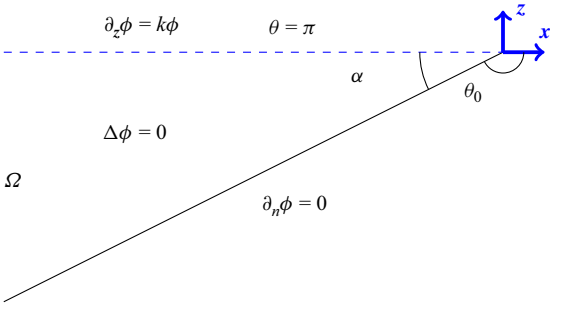


Figure 1. Schematic diagram showing the equations of motion and boundary conditions.

Due to the problem geometry, it is convenient to consider it in polar coordinates

$$x = r\cos\theta, \quad z = r\sin\theta, \tag{2.3}$$

with the origin at the corner where the fluid surface and the beach meet. Along the beach, the Neumann boundary condition of no flow applies, so that

$$\frac{\partial}{\partial n}\phi(r,\theta)\big|_{\theta=\theta_0} = 0, \tag{2.4}$$

where n is the outer normal to the boundary. In accordance with the linearised theory, at the water surface, we define the surface displacement by $\zeta(t, x)$. The kinematic condition

$$\partial_z\phi = \partial_t\zeta, \quad z = 0, \tag{2.5}$$

and the dynamic condition (Mei 1989)

$$\partial_t\phi + g\zeta = 0, \quad z = 0, \tag{2.6}$$

where g is the gravitational acceleration. In the frequency domain, assuming all functions are proportional to $\mathrm{e}^{-\mathrm{i}\omega t}$, these conditions become

$$\partial_z\phi = k\phi, \quad z = 0, \tag{2.7}$$

where $k = \omega^2/g$ and ω is the angular frequency.

This problem has been addressed using the complex analysis in Lewy (1946), Stoker (1947), Isaacson (1950) and Peters (1950), while Ehrenmark (1987, 1989) found a closed form solution representation using Mellin transform. In the first two papers, exact solutions have been constructed for domains with specific angles, respectively, $\theta_0 = \pi + \pi/(2m)$ and $\theta_0 = \pi + \pi p/(2m)$ ($p < 2m$, where p and m are natural numbers), while the latter extended the method to consider an arbitrary domain $\pi < \theta_0 \leqslant 2\pi$. Note that, in their analysis, they measure the angle differently: $0 < \theta < \alpha \leqslant \pi$ ($\theta_0 = \alpha + \pi$).

It was shown that this linear homogeneous problem has a non-trivial solution that describes sinusoidal waves along the water surface at infinity ($r \to \infty$) and it is bounded as $r \to 0$ (see figure 1) (we note that the classic papers mentioned above, in addition to the regular solution considered in this paper, also discussed singular solutions; we will consider those in a separate paper)

$$\phi(r,\theta) = \phi_0 + \phi_1 r^{\gamma_0} + O\left(r^{\gamma_0+\delta}\right), \quad r \to 0, \quad \pi < \theta \leqslant \theta_0 \leqslant 2\pi, \tag{2.8}$$

Here, $\phi_j = \phi_j(\theta_0)$ and $0 < \gamma_0(\theta_0) \leqslant 1$ are to be determined, while $\delta > 0$ is a small number.

To ensure the uniqueness of the solution, we require the following asymptotic estimate is valid:

$$\phi(x,z) = e^{ikx}e^{kz} + R\,e^{-ikx}e^{kz} + o(1), \quad x \to -\infty. \tag{2.9}$$

https://doi.org/10.1017/jfm.2026.12121 Published online by Cambridge University Press

Here, R is the complex reflection coefficient that in this case represents a shift in the mode between the incident and the reflected waves (which are the first and second terms in (2.9), respectively). For the regular solution, energy conservation gives $|R| = 1$. Moreover, for those analytical solutions presented in Lewy (1946), the remainder (the $o(1)$ term in (2.9)) exponentially decays at infinity and represents evanescent waves. However, when considering the obtuse beach angle ($\pi/2 < \alpha < \pi$) or dock problem ($\alpha = \pi$) it is considered that the decay is slower (algebraic).

We do not require any of these facts (knowledge of the reflection coefficient, R, or the rate of decay) and will receive the proper results in due course of our analysis.

REMARK 1. *Note that, for the vertical slope ($\theta_0 = 3\pi/2$, or equivalently, $\alpha = \pi/2$) the regular solution is trivial and represents a well-known standing wave*

$$\phi(x, z) = e^{ikx}e^{kz} + e^{-ikx}e^{kz} = 2e^{kz}\cos kx, \tag{2.10}$$

thus, $R = 1$ in this case.

In the next subsection, we reformulate the above problem using the Mellin transform, paying particular attention to the properties of analytical function that represents the Mellin image of the potential $\phi(r, \pi)$ along the surface of the free water. Those properties are natural and are crucial in understanding our further transformations.

2.2. *Transformation of the problem using Mellin transform*

Following Ehrenmark (1987), we apply the Mellin transform, defined as

$$\mathcal{M}\{\phi\}(s, \theta) \equiv \tilde{\phi}(s, \theta) = \int_0^\infty r^{s-1}\phi(r, \theta)\,\mathrm{d}r \tag{2.11}$$

to the governing (2.2) and the boundary conditions (2.4) and (2.7). Here s is the Mellin transform variable, a complex number belonging to a domain to be discussed later. This leads to the trivial ordinary differential equation

$$\tilde{\phi}_{\theta\theta} + s^2\tilde{\phi} = 0. \tag{2.12}$$

According to estimates (2.8) and (2.9), the solution sought does not belong to a classic functional space of this transform. Thus, we should operate in a space of distribution (Zemanian 1987). This is not difficult in this case due to the smoothness of the solution inside the domain but requires the respective justifications.

To avoid this route, we consider a regularised solution to the problem with a slightly deformed asymptotic estimate at infinity

$$\phi(r, \pi) = e^{-ikr}e^{-\epsilon r} + R\,e^{ikr}e^{-\epsilon r} + O\big(r^{-\gamma_\infty}\big), \quad r \to \infty, \tag{2.13}$$

where $\epsilon > 0$ can later be taken to zero to allow both the incident and a reflected wave to be present. Again, the parameters R and $\gamma_\infty > 0$ are considered unknown.

As a result, we expect that the Mellin image, $\tilde{\phi}(s, \theta)$, is an analytic function in the strip $0 < \mathrm{Re}\, s < \gamma_\infty$ for any $\pi < \theta \leqslant \theta_0$ and $\pi < \theta_0 \leqslant 2\pi$.

Moreover, *a priori* estimates (2.8) and (2.13) suggest that the function can possess simple poles

$$\tilde{\phi}(s, \theta) \sim \frac{\phi_0}{s} + O(1), \quad s \to 0, \tag{2.14}$$

while

$$\tilde{\phi}(s, \theta) \sim \frac{\phi_1}{s + \gamma_0} + O(1), \quad s \to -\gamma_0, \tag{2.15}$$

https://doi.org/10.1017/jfm.2026.12121 Published online by Cambridge University Press

and the function $\tilde{\phi}(s,\theta)$ can be analytically extended into the strip

$$-\gamma_0-\delta<\mathrm{Re}s<\gamma_\infty, \tag{2.16}$$

where $\delta>0$.

REMARK 2. *We expect the following for the unknown parameter that defines the estimate of the solution at zero and infinity:*

$$\begin{aligned}&\gamma_0=1,\quad \gamma_\infty=\infty, && \text{when}\quad 0<\alpha<\pi/2,\\ &0<\gamma_0(\alpha)<1,\quad \gamma_\infty(\alpha)>1, && \text{when}\quad \pi/2<\alpha<\pi.\end{aligned} \tag{2.17}$$

In what follows, we refer to the unknown strip (2.16), specifying the parameters when appropriate.

Finally, we observe that the function $\tilde{\phi}(it,\theta)$ should decay faster than any inverse polynomial as $t\to\pm\infty$, due to the smoothness of the original solution.

Using the boundary condition (2.4) we can conclude that

$$\tilde{\phi}(s,\theta)=A(s)\cos(\theta-\theta_0)s, \tag{2.18}$$

or

$$\phi(r,\theta)=\frac{1}{2\pi i}\int_{-i\infty+\eta}^{i\infty+\eta}A(s)\cos\big(s(\theta-\theta_0)\big)r^{-s}ds,\quad 0<\eta<\gamma_\infty. \tag{2.19}$$

An equivalent representation of (2.19) is

$$\phi(r,\theta)=\frac{1}{2\pi i}\int_{-i\infty+\eta}^{i\infty+\eta}\tilde{\phi}(s,\pi)\frac{\cos s(\theta-\theta_0)}{\cos s(\pi-\theta_0)}r^{-s}ds, \tag{2.20}$$

demonstrating that the integration path can be shifted to the left, revealing the asymptotic estimate (2.8).

In the next section, we formulate a functional equation (2.33) for an auxiliary function $w(r)$ (its Mellin image is an analytical function $\tilde{w}(s)$) that preserves the properties of the potential along the free water surface ($\theta=\pi$) and decays at infinity (thus the incident and reflected waves are participated in the analysis separately in their analytical forms).

2.3. *Transforming the original problem to a functional equation*

Let us introduce a representation of the solution on the surface $z=0$ in the form

$$\phi(r,\pi)=U_\epsilon(r)+w(r),\quad U_\epsilon(r)=e^{-ikr}e^{-\epsilon r}+R\,e^{ikr}e^{-\epsilon r}, \tag{2.21}$$

where U_ϵ represents the incident and reflected wave contribution to the surface potential. We can write (compare with (2.8) and (2.9)) we can write

$$w(r)=w_0+w_1r^{\gamma_1}+O(r^{\gamma_1+\delta}),\quad r\to 0, \tag{2.22}$$

$$w(r)=w_\infty r^{-\gamma_\infty}+O(r^{-\gamma_\infty-\delta}),\quad r\to\infty, \tag{2.23}$$

where

$$\phi_0=1+R+w_0,\quad \gamma_1=\min\{1,\gamma_0\}>0, \tag{2.24}$$

and both constants R and w_0 are unknown at this stage and will be determined later.

Note that determining the function $w(r)$ is enough to solve the original problem due to (2.21) and the representation (2.20).

https://doi.org/10.1017/jfm.2026.12121 Published online by Cambridge University Press

We emphasise that both functions ϕ and w actually depend on the parameter ϵ (that is, $\phi = \phi_\epsilon$ and $w = w_\epsilon$), while the solution to the original problem will be obtained in the limit $\epsilon \to 0$. For the sake of clarity, we will omit the additional subscripts and simply indicate where the limit is taken to recover the solution.

Next, we compute

$$\tilde{\phi}(s, \pi) = \tilde{w}(s) + \tilde{U}_\epsilon(s). \tag{2.25}$$

Moreover (compare with (2.22)),

$$\tilde{w}(s) = \frac{w_0}{s} + O(1), \quad s \to 0, \tag{2.26}$$

$$\tilde{w}(s) = \frac{w_1}{s + \gamma_0} + O(1), \quad s \to -\gamma_0, \tag{2.27}$$

and there are no other poles of the function in the strip $-\gamma_1 - \delta < \mathrm{Re}s < \gamma_\infty$.

REMARK 3. *In the following, we assume*

$$\gamma_1 + \gamma_\infty + \delta > 1, \tag{2.28}$$

that will be justified in due course.

As a result, functions $s\tilde{w}(s)$ and $\tilde{w}(s+1)$ are analytical in the common strip

$$-\gamma_1 - \delta < \mathrm{Re}s < \gamma_\infty - 1, \tag{2.29}$$

having no poles except at those points mentioned in (2.26) and (2.27), and they both decay at infinity as

$$\tilde{w}(s) = O(|s|^{-\beta}), \quad |\mathrm{Im}s| \to \infty. \tag{2.30}$$

Here, $\beta > 0$ is an arbitrary constant.

REMARK 4. *In the following, the information in (2.30) is crucial.*

The other term in (2.25) can be computed exactly to read

$$\tilde{U}_\epsilon(s) = \frac{\Gamma(s)}{(\epsilon + ik)^s} + \frac{\Gamma(s)}{(\epsilon - ik)^s} R. \tag{2.31}$$

Note that the latter is analytical in the strip $0 < \mathrm{Re}s < b$ ($b > 0$ is an arbitrary value) and $\tilde{U}_\epsilon(s)$ has a simple pole at zero

$$\tilde{U}_\epsilon(s) \sim \frac{1 + R}{s}, \quad s \to 0, \tag{2.32}$$

while $\tilde{U}_\epsilon(s)$ has a simple pole at the point $s = -1$ (related to the behaviour of the gamma function). Both functions $\tilde{U}_\epsilon(s)$ and $\tilde{U}_\epsilon(s+1)$ decay at infinity faster than any inverse polynomial of s ($|\mathrm{Im}s| \to \infty$) provided $\epsilon > 0$.

Applying the Mellin transform to the remaining unused condition on the free water surface (2.7), we obtain a functional equation

$$s\tilde{w}(s) \tan\big(s(\pi - \theta_0)\big) - k\tilde{w}(s+1) = \tilde{f}_\epsilon(s), \tag{2.33}$$

valid in the strip (2.29) where

$$\tilde{f}_\epsilon(s) = -s\tilde{U}_\epsilon(s) \tan(s(\pi - \theta_0)) + k\tilde{U}_\epsilon(s+1). \tag{2.34}$$

Let us now pass to the limit $\epsilon \to 0$

$$\tilde{U}_0(s) = \lim_{\epsilon \to 0} \tilde{U}_\epsilon(s) = \frac{\Gamma(s)}{k^s} \left((1 + R) \cos \frac{\pi s}{2} - i(1 - R) \sin \frac{\pi s}{2} \right), \tag{2.35}$$

https://doi.org/10.1017/jfm.2026.12121 Published online by Cambridge University Press

while

$$\tilde{U}_0(s+1) = \frac{\Gamma(1+s)}{k^{s+1}}\left(-(1+R)\sin\frac{\pi s}{2} - i(1-R)\cos\frac{\pi s}{2}\right). \tag{2.36}$$

This allows us to compute a limiting function from (2.34)

$$\tilde{f}_0(s) = -\frac{\Gamma(s+1)}{k^s}\left((1+R)\frac{\sin s\left(\frac{3\pi}{2}-\theta_0\right)}{\cos s(\pi-\theta_0)} + i(1-R)\frac{\cos s\left(\frac{3\pi}{2}-\theta_0\right)}{\cos s(\pi-\theta_0)}\right). \tag{2.37}$$

Note that $\tilde{f}_0(s)$ is an analytical meromorphic function in the strip containing the origin $s=0$

$$-\min\left\{1, \frac{\pi}{2(\theta_0-\pi)}\right\} < \mathrm{Re}s < \frac{\pi}{2(\theta_0-\pi)}, \tag{2.38}$$

and can be considered in any wider strip where it has poles related to the gamma function ($s=-1,-2,\ldots$) and the trigonometric functions ($s=((\pi+2\pi j)/(2(\theta_0-\pi)))$, $j=\pm1,\pm2,\ldots$). Moreover, for any $\theta_0>\pi$, $\tilde{f}_0(s)$ exponentially decays at infinity within the strip. In this way, we have justified our notation. Indeed, there exists a function $f_0(r)$ such that $\tilde{f}_0(s)=\mathcal{M}[f_0](s)$.

Rewriting (2.33) in the form

$$s\tilde{w}(s) = \frac{k\tilde{w}(s+1)+\tilde{f}_0(s)}{\tan\left(s(\pi-\theta_0)\right)}, \tag{2.39}$$

analysing it as well as (2.33) we conclude in the worst-case scenario that

$$\gamma_0 = \min\left\{1, \frac{\pi}{2(\theta_0-\pi)}\right\}, \quad \gamma_\infty = 1+\frac{\pi}{2(\theta_0-\pi)}, \tag{2.40}$$

thus the assumption (2.28) is always satisfied. Note that the strip (2.29) can be wider (for example, if some of the constants w_1 or w_∞ vanishes). Moreover, we can always analytically extend the equation in any finite strip where the equation can have isolated poles. Finally, by analysing (2.39) near the point $s=0$, we conclude

$$k\tilde{w}(s+1)+k\tilde{U}_0(s+1) \sim s(\pi-\theta_0)w_0, \quad s\to 0. \tag{2.41}$$

Note that

$$\tilde{w}(1) = -\tilde{U}_0(1) = \frac{i(1-R)}{k}, \tag{2.42}$$

represents the solvability condition for the Laplace equation in the wedge domain with the Neumann boundary condition on the sides on the edges (see figure 1).

From this point on, the functions $w(r)$ and $\tilde{w}(s)$ are related to the original solution obtained in the limit $\epsilon\to 0$.

While the Mellin-transform framework employed up to this point can naturally share elements with the analyses presented in Ehrenmark's papers, the subsequent development introduces a distinct formulation that diverges from his methodology. That is, we are now going to further transform (2.33) to produce another functional equation (2.48). The second equation differs from the first one in that all the coefficients in front of the unknown functions have a finite, non-zero limit as their argument tends to infinity along the imaginary axis in the complex plane. This, in turn, allows us to transform the latter to an integral equation with a kernel that admits a good behaviour along the real axis.

https://doi.org/10.1017/jfm.2026.12121 Published online by Cambridge University Press

2.4. *Transformation of functional equation (2.33)*

To achieve the goal, we use a similar line of reasoning as in Mishuris (2001) by looking for a solution of (2.33) in terms of a new function $p(r)$

$$\tilde{w}(s+1) = -\frac{1}{k^{s+1}}\Gamma(s+1)\sin\frac{\pi s}{2}\left(\tilde{p}(s+1) - \frac{A}{\sin\dfrac{\pi s}{2}}\right), \tag{2.43}$$

$$\tilde{w}(s) = \frac{1}{k^{s}}\Gamma(s)\cos\frac{\pi s}{2}\left(\tilde{p}(s) + \frac{A}{\cos\dfrac{\pi s}{2}}\right), \tag{2.44}$$

where function $\tilde{p}(s)$ is the Mellin transform of the unknown function $p(r)$ which is analytic on the same strip with some change in behaviour near the points $s = 0, \pm 1$, while the constant A will be defined later.

REMARK 5. *Note that, for any real t,*

$$|\Gamma(it)| = \sqrt{\frac{\pi}{t\sinh\pi t}}, \tag{2.45}$$

and thus the function $\tilde{p}(s)$ introduced in (2.44) behaves at infinity in a manner similar to the original function $\tilde{w}(s)$

$$\frac{\tilde{w}(it)}{\tilde{p}(it)} = O(t^{-1/2}), \quad t \to \pm\infty \tag{2.46}$$

thus both of them should simultaneously decay at infinity or

$$\lim_{t\to\pm\infty}\tilde{p}(it) = 0 \tag{2.47}$$

(compare this with the assumption (2.30)). Lastly, the function $\tilde{p}(s)$, in contrast to $\tilde{w}(s)$, does not have a pole at the point $s = 0$.

Substituting (2.43)–(2.44) into (2.33) we arrive at a new functional equation

$$\tan\big(s(\theta_0 - \pi)\big)\tilde{p}(s) - \tan\frac{\pi s}{2}\tilde{p}(s+1) = \tilde{f}_1(s), \tag{2.48}$$

in the strip

$$-1 < \mathrm{Re}s < \frac{\pi}{2(\theta_0 - \pi)}, \tag{2.49}$$

where the functions $\tilde{p}(s)$ and $\tilde{p}(s+1)$ do not have any poles. The function $\tilde{f}_1(s)$ is given by

$$\tilde{f}_1(s) = -\frac{1}{\cos\dfrac{\pi s}{2}}\left(\frac{k^s}{\Gamma(s+1)}\tilde{f}_0(s) + A\left(\tan\big(s(\theta_0 - \pi)\big) + 1\right)\right), \tag{2.50}$$

the constant A can now be evaluated so as to ensure that $\tilde{p}(s)$ is analytic at $s = 1$ (compare (2.26), (2.41), (2.36) and (2.44))

$$A = i(1 - R), \quad \tilde{p}(0) + A = w_0. \tag{2.51}$$

To summarise the rationale behind the substitution (2.43), we note that the new unknown function $\tilde{p}(s)$ (i) exhibits the same asymptotic behaviour at infinity within the strip of

https://doi.org/10.1017/jfm.2026.12121 Published online by Cambridge University Press

analyticity as $\tilde{w}(s)$, (ii) does not possess poles in a wider strip (does not have the pole at $s=0$) and (iii) appears in the functional equation (2.33) without algebraically growing coefficients in front of the unknowns $\tilde{p}(s)$ and $\tilde{p}(s+1)$. This allows us to apply the inverse Mellin transform to the equation using a Fubini-type theorem and avoids the need to work in distributional spaces. Finally, we have eliminated the gamma function from the right-hand side of the functional equation (2.33) (compare (2.37) and (2.50)).

We observe that the right hand side of (2.48) can be split into the sum

$$\tilde{f}_1(s) = (1+R)\,\tilde{f}_1^{(1)}(s) + i(1-R)\,\tilde{f}_1^{(2)}(s), \tag{2.52}$$

where

$$\tilde{f}_1^{(1)}(s) = \frac{\sin s\left(\dfrac{3\pi}{2}-\theta_0\right)}{\cos s(\pi-\theta_0)\cos\dfrac{\pi s}{2}},$$
$$\tilde{f}_1^{(2)}(s) = \frac{\cos s\left(\dfrac{3\pi}{2}-\theta_0\right)}{\cos s(\pi-\theta_0)\cos\dfrac{\pi s}{2}} - \frac{\tan(s(\theta_0-\pi))+1}{\cos\dfrac{\pi s}{2}}. \tag{2.53}$$

This representation allows us to search for the solution of (2.48) in a form similar to (2.52)

$$\tilde{p}(s) = (1+R)\tilde{p}^{(1)}(s) + i(1-R)\tilde{p}^{(2)}(s), \tag{2.54}$$

where each of the functions with the subscript $j=1,2$ satisfy the respective equation

$$\tan s(\theta_0-\pi)\tilde{p}^{(j)}(s) - \tan\frac{\pi s}{2}\tilde{p}^{(j)}(s+1) = \tilde{f}_1^{(j)}(s). \tag{2.55}$$

Note that functions $f_1^{(j)}(s)$ can be estimated at infinity inside the analyticity strip

$$\tilde{f}_1^{(j)}(s) = O(e^{q|s|}), \quad \mathrm{Im}s \to \pm\infty, \tag{2.56}$$

with $q = |3\pi/2-\theta_0| - \theta_0 + \pi/2 \leqslant -\pi$.

Moreover,

$$\tilde{f}_1^{(2)}(s) = -s(\theta_0-\pi) + O(s^2), \quad \tilde{f}_1^{(1)}(s) = s\left(\frac{3\pi}{2}-\theta_0\right) + O(s^3), \quad s\to 0. \tag{2.57}$$

Thus, since $\tilde{p}^{(j)}(s)$ is analytic near the point $s=0$, and the same happens at $s=1$, the left-hand side of (2.55) vanishes as $s\to 0$.

As a result of this subsection, we have arrived at two independent functional equations (2.55) that are essentially the same (having only different right-hand sides). When we further transform them into integral equations with fixed-point singularities at the ends of the integration path, we will observe that the solution may possess an additional unwanted property. Namely, they might have a singularity $(r-1)^{-1}$, as $r\to 1$ and thus their analysis in the classic functional spaces natural for such equations cannot be performed. We try to highlight the problem differently. Note that the auxiliary function $\tilde{p}(s)$ has to satisfy the additional condition (2.47), while the functions $\tilde{p}^{(j)}(s)$ do not necessarily need to possess such properties. For example, it is easy to observe that any of the assumptions

$$\tilde{p}^{(j)}(it) \to C_j, \quad \text{or} \quad \tilde{p}^{(j)}(it) \to C_j\tan(it), \quad t\to\pm\infty \tag{2.58}$$

do not contradict (2.55) and this fact should be taken into account.

https://doi.org/10.1017/jfm.2026.12121 Published online by Cambridge University Press

2.5. *Further transformation of functional equations (2.55)*

To address this fact, we represent the unknown solutions as follows:

$$p^{(j)}(r) = \frac{2d_j}{\pi}\left(\frac{r}{r^2-1} - \frac{r}{r^2+1}\right) + p_*^{(j)}(r), \tag{2.59}$$

or

$$\tilde{p}^{(j)}(s) = d_j\left(\tan\frac{\pi s}{2} - \frac{1}{\cos\dfrac{\pi s}{2}}\right) + \tilde{p}_*^{(j)}(s), \tag{2.60}$$

$$\tilde{p}^{(j)}(s+1) = -d_j\left(\cot\frac{\pi s}{2} - \frac{1}{\sin\dfrac{\pi s}{2}}\right) + \tilde{p}_*^{(j)}(s+1),$$

where functions $p_*^{(j)}(r)$ are regular near the point $r = 1$ or, equivalently,

$$\tilde{p}_*^{(j)}(s) \to 0, \quad |\mathrm{Im} s| \to \infty. \tag{2.61}$$

Thus, instead of two functions $\tilde{p}^{(j)}(s)$, we need to find two constants d_j and functions $\tilde{p}_*^{(j)}(s)$. Note that $\tilde{p}^{(j)}(s)$ from (2.60) generally do not decay at infinity. To guarantee the decay of the function $\tilde{p}(s)$ (compare (2.47), (2.54) and (2.61)) we put

$$(1+R)d_1 + i(1-R)d_2 = 0, \tag{2.62}$$

that, in turn, defines the reflection coefficient R. We would like to underline here that nothing at this stage shows that condition $|R| = 1$ is valid, since the values of the (complex) constants d_j are unknown.

The final solution $\tilde{p}(s)$ takes the form (note that $p_*^{(j)}(s)$ and $p^{(j)}(s)$ from (2.54) are different)

$$\tilde{p}(s) = (1+R)\tilde{p}_*^{(1)}(s) + i(1-R)\tilde{p}_*^{(2)}(s). \tag{2.63}$$

As a result, the functional equations (2.55), written in terms of the functions $\tilde{p}_*^{(j)}(s)$, take similar forms to the other right-hand sides and while their solutions are bounded as $s \to \infty$ inside the analyticity strip (2.49)

$$\tan s(\theta_0 - \pi)\tilde{p}_*^{(j)}(s) - \tan\frac{\pi s}{2}\tilde{p}_*^{(j)}(s+1) = \tilde{f}_{\clubsuit}^{(j)}(s), \quad j = 1, 2, \tag{2.64}$$

where

$$\tilde{f}_{\clubsuit}^{(j)}(s) = \tilde{f}_1^{(j)}(s) - d_j\tilde{f}_1^{(2)}(s). \tag{2.65}$$

After this preparatory work, we are ready to evaluate the integral equations that possess enough flexibility (additional parameters) to eliminate that possible singular behaviour at the point $r = 1$.

2.6. *Transformation of functional equations (2.64) to integral equations*

We now divide (2.64) by $\tan(\pi s/2)$ and observe that

$$\cot\frac{\pi s}{2}\tan s(\theta_0 - \pi) = 1 - \tilde{n}_0(s), \tag{2.66}$$

https://doi.org/10.1017/jfm.2026.12121 Published online by Cambridge University Press

where

$$\tilde{n}_0(s) = \frac{\sin s\left(\dfrac{3\pi}{2} - \theta_0\right)}{\sin\dfrac{\pi s}{2}\cos s(\theta_0 - \pi)}. \tag{2.67}$$

This allows us, by applying the inverse Mellin transform, to rewrite equations (2.64) in the form

$$(1-r)p_*^{(j)}(r) - \mathcal{N}[p_*^{(j)}](r) = f_*^{(j)}(r) \equiv \frac{1}{2\pi i}\int_{-i\infty+\eta}^{i\infty+\eta} \frac{\tilde{f}_{\clubsuit}^{(j)}(s) r^{-s}\,\mathrm{d}s}{\tan(\pi s/2)}, \tag{2.68}$$

where $\eta > 0$ is an arbitrary value such that $\eta < \min\{\gamma_1, \gamma_\infty - 1\}$, where γ_1 and γ_∞ were evaluated in (2.40). Here, the integral operator $\mathcal{N}$ is

$$\mathcal{N}[u](r) = \int_0^\infty n_0(t/r)u(t)\frac{\mathrm{d}t}{t}, \tag{2.69}$$

and its kernel, $n_0(r)$, defined in (2.67) can be simplified for computations

$$n_0(r) = \frac{1}{\pi}\int_0^\infty \frac{\sinh(3\pi/2 - \theta_0)\xi\,\cos(\xi\log r)}{\sinh(\pi\xi/2)\cosh(\theta_0 - \pi)\xi}\mathrm{d}\xi. \tag{2.70}$$

To our knowledge, there are no closed analytical representations for this function for an arbitrary value of θ (see Gradshteyn & Ryzhik 2014).

Since the unknown function $p_*^{(j)}(r)$ should be smooth along the positive part of the real axis, we additionally require the following two conditions to be valid to eliminate the possible singularity at the point $r = 1$:

$$\mathcal{N}[p_*^{(j)}](1) + f_*^{(j)}(1) = 0. \tag{2.71}$$

These, in turn, define the two still unknown constants d_j.

The right-hand sides of (2.68) can be further evaluated

$$f_*^{(1)}(r) \equiv \frac{1}{2\pi i}\int_{-i\infty+\eta}^{i\infty+\eta}\left(\tilde{f}_1^{(1)}(s) - d_1\tilde{f}_1^{(2)}\right)\frac{r^{-s}\mathrm{d}s}{\tan(\pi s/2)} = n_0(r) - d_1 n_d(r), \tag{2.72}$$

where

$$n_d(r) = \frac{1}{2\pi i}\int_{-i\infty}^{i\infty}\left(\frac{1}{\sin\dfrac{\pi s}{2}}\left(\frac{\cos s\left(\dfrac{3\pi}{2} - \theta_0\right)}{\cos s(\theta_0 - \pi)} - 1\right) - \frac{\tan s(\theta_0 - \pi)}{\sin\dfrac{\pi s}{2}}\right) r^{-s}ds, \tag{2.73}$$

while

$$f_*^{(2)}(r) \equiv \frac{1}{2\pi i}\int_{-i\infty+\eta}^{i\infty+\eta}\left(\tilde{f}_1^{(2)}(s) - d_2 f_1^{(2)}(s)\right)\frac{r^{-s}\mathrm{d}s}{\tan(\pi s/2)} = (1-d_2)n_d(r). \tag{2.74}$$

Note that for $\alpha \neq \pi/2$, any natural $j = 1, 2, 3, \ldots$, and $l = 0, d$

$$t^j\frac{\mathrm{d}^j}{\mathrm{d}t^j}n_l(t) = O(t^{\beta_*}), \quad t \to 0, \quad t^j\frac{\mathrm{d}^j}{\mathrm{d}t^j}n_l(t) = O(t^{-\beta_*}), \quad t \to \infty, \tag{2.75}$$

where

$$\beta_* = \min\left\{1, \frac{\pi}{2\alpha}\right\} = \min\left\{1, \frac{\pi}{2(\theta_0 - \pi)}\right\}. \tag{2.76}$$

https://doi.org/10.1017/jfm.2026.12121 Published online by Cambridge University Press

Then, (2.68) read (introducing the operator $\mathcal{B}$)

$$\mathcal{B}[p_*^{(j)}](r) \equiv (1-r)p_*^{(j)}(r) - \mathcal{N}[p_*^{(j)}](r) = n_j(r) - d_j n_d(r), \quad j = 1, 2, \tag{2.77}$$

where $n_1(r) = n_0(r)$, $n_2(r) = n_d(r)$, while the respective conditions (2.71) read

$$\mathcal{N}[p_*^{(j)}](1) + n_j(1) = d_j n_d(1). \tag{2.78}$$

Note that since

$$n_d(1) = -\frac{1}{\pi}\int_0^\infty \frac{\tanh t(\theta_0 - \pi)}{\sinh \dfrac{\pi t}{2}} \mathrm{d}t < 0, \tag{2.79}$$

conditions (2.78) make sense. However, one can expect that for small values of the angle $\alpha = \theta_0 - \pi$, computations would be challenging (not a surprise, as here the equation of shallow water should take over).

Statement 1. For almost all $0 < \alpha \le \pi$, each of equation (2.77), with the corresponding condition (2.78), has a unique smooth solution on the open positive half-axis that satisfies the following estimate at the ends of the interval:

$$p_*^{(j)}(r) \sim p_0^{(j)} r^{\beta_0}, \quad r \to 0, \quad p_*^{(j)}(r) \sim p_\infty^{(j)} r^{-\beta_\infty}, \quad r \to \infty. \tag{2.80}$$

The exceptional angles are discussed in Remarks 9 and 10.

The idea of the proof. Details on the analysis of integral equations with fixed-point singularities of that kind can be found in Mishuris (1995*b*). Moreover, the equation can be solved numerically by the respective projection methods (Gokhberg & Feldman 1974).

Although the behaviour at infinity is easy to justify since $\beta_\infty = 1 + \beta_*$ (see (2.76)), the other estimate is more difficult as it also involves analysis of the symbol of operator $\mathcal{B}$ (see Mishuris 1995*b*). Indeed, the behaviour at the zero point is defined by the zeros of the function $1 - \tilde{n}_0(s)$ that is the symbol of the integral operator $\mathcal{B}$ defined on the left side of (2.77). Note that, since $1 - n_0(0) = 2(\theta_0 - \pi)/\pi > 0$ (compare with (2.67)), it follows that $1 - \tilde{n}_0(it) > 0$ for any real t. The zero of the symbol possessing the minimal real part inside the analyticity strip is real, and the exponent in the asymptotic estimate at the zero point, $\beta_0 > 0$, is defined from the equation: $\sin \beta_0(\theta_0 - \pi)\cos(\pi\beta_0/2) = 0$, or $\beta_0 = \min\{1, \pi/(\theta_0 - \pi)\}$. On the other hand, the right-hand side of (2.77) (and the operator involved) can be estimated, as (2.75) defines the leading-order term that explains (2.80). As a result, we conclude that $\beta_0 = \beta_*$. In other words, the functions $\tilde{p}_*^{(j)}(s)$ are analytical at are analytical in the strip

$$-\min\{\beta_0, \beta_*\} < \Re s < \min\{1 + \beta_*, \beta_\infty\}. \tag{2.81}$$

REMARK 6. *If we take $d_2 = 1$, then (2.77) has a trivial solution, $p_*^{(2)}(r) \equiv 0$. Since the solution is unique, the only equation we need to solve is that of $j = 1$.*

REMARK 7. *Note that both the parameter d_1 and the respective smooth solution $p^{(1)}(r, d_1)$ of the remaining integral equation are real. The reflection coefficient should then be found from (2.62)*

$$R = -\frac{d_1 + id_2}{d_1 - id_2} = \frac{1 - id_1}{1 + id_1}, \tag{2.82}$$

noting that $d_2 = 1$. This shows that the reflection coefficient indeed satisfies the condition $|R| = 1$. Moreover, the phase shift ν is related to the reflection coefficient

$$R = e^{2i\nu}, \quad \tan\nu = -d_1. \tag{2.83}$$

https://doi.org/10.1017/jfm.2026.12121 Published online by Cambridge University Press

REMARK 8. *Note that the values β_0 and β_∞ in the asymptotics (2.80) are computed above from the worst-case scenario, as the constants $p_0^{(1)}$ and $p_\infty^{(1)}$ can be zero and the next asymptotic terms should be analysed. These constants can be directly computed from the numerical procedure since the asymptotic is very pronounced (see figure 2, for example). However, they can also be computed as an integral functionals on the solution allowing for additional accuracy control. The respective formulas may depend on the value of the angle α. The respective analysis is provided in Appendix A.*

Now, when we have proved the solvability of the integral equations, we can reconstruct the solution of the original problem described in § 2.1.

2.7. *Reconstruction of the original solution*

Taking into account (2.35), (2.44) and (2.51) we have

$$\tilde{\phi}(s,\pi) = \tilde{U}_0(s) + \frac{1}{k^s}\Gamma(s)\cos\frac{\pi s}{2}\left(\tilde{p}(s) + \frac{A}{\cos\dfrac{\pi s}{2}}\right)$$
$$= \frac{\Gamma(s)}{k^s}\left((1+R)\cos\frac{\pi s}{2} - (1-R)i\sin\frac{\pi s}{2} + \cos\frac{\pi s}{2}\tilde{p}(s) + i(1-R)\right). \quad (2.84)$$

We can now observe that for any $k > 0$

$$\int_0^\infty x^{s-1}\sin kx\,\mathrm{d}x = k^{-s}\Gamma(s)\sin\frac{\pi s}{2}, \quad -1 < \mathrm{Re}s < 1,$$
$$\int_0^\infty x^{s-1}\cos kx\,\mathrm{d}x = k^{-s}\Gamma(s)\cos\frac{\pi s}{2}, \quad 0 < \mathrm{Re}s < 1. \quad (2.85)$$

Applying the inverse Melling transform to (2.20) (for $\theta = \pi$) and any $0 < \eta < \beta_*$ to (2.84), while using the convolution theorem for the Melin transform (see, for example, Zemanian (1987)), allows us to reconstruct the potential on the water surface. As discussed in (2.63), $p(r)$ is represented as a sum of two terms; therefore,

$$\phi(r,\pi) = (1+R)\big(\cos kr + T(kr)\big) - i(1-R)\big(\sin kr - e^{-kr}\big). \quad (2.86)$$

Here we define ($\eta > 0$)

$$T(y) = \frac{1}{2\pi i}\int_{-i\infty+\eta}^{i\infty+\eta}\Gamma(s)\cos\frac{\pi s}{2}\tilde{p}_*^{(1)}(s)y^{-s}\mathrm{d}s = \int_0^\infty \cos\left(\frac{y}{t}\right)p_*^{(1)}(t)\,\frac{\mathrm{d}t}{t}. \quad (2.87)$$

Note that solution (2.86) can be written in the form

$$\phi(r,\pi) = 2e^{i\nu}\big(\cos(kr+\nu) + T(kr)\cos\nu + e^{-kr}\sin\nu\big). \quad (2.88)$$

The value of the potential at the vertex is computed as follows:

$$\phi(0,\pi) = 2e^{i\nu}\big(\big(1+\tilde{p}_*^{(1)}(0)\big)\cos\nu + \sin\nu\big), \quad (2.89)$$

while the maximal amplitude of the potential at infinity is

$$|\phi(\infty,\pi)| = \lim_{r\to\infty}\max_{[r,r+2\pi/k]}|\phi(\cdot,\pi)| = 2. \quad (2.90)$$

The following two statements concerning phase shift and run-up can be found, for example, in Sretensky (1977) and Stoker (2019) when the author discusses the known results for the case of discrete solutions $\alpha = \pi/(2m)$, $m = 1, 2, \ldots$. On the other hand, a

https://doi.org/10.1017/jfm.2026.12121 Published online by Cambridge University Press

common expectation noted in most of the classic works is that the formulas for discrete values are valid in the general case (arbitrary angle) due to continuity arguments. We formulate these statements using our notation and verify their validity numerically using our approach.

Statement 2. The reflection coefficient (2.83) for arbitrary $0 < \alpha \leqslant \pi$ $(\theta_0 = \alpha + \pi)$ can be calculated by the formula

$$R = e^{\frac{i\pi(\pi-2\alpha)}{4\alpha}} = e^{\frac{i\pi(3\pi-2\theta_0)}{4(\theta_0-\pi)}}, \quad \nu = \frac{\pi(\pi-2\alpha)}{8\alpha}. \tag{2.91}$$

Statement 3. The following equation is valid for arbitrary $0 < \alpha \leqslant \pi$ $(\theta_0 = \alpha + \pi)$:

$$\frac{1}{2}\, e^{-i\nu}\phi(0,\pi) = \sqrt{\frac{\pi}{2\alpha}} = \sqrt{\frac{\pi}{2(\theta_0-\pi)}}. \tag{2.92}$$

Since Statements 2 and 3 have been theoretically proven for $\alpha = \pi/(2m)$, we use such cases to additionally verify the accuracy of our computations.

COROLLARY 1. *We can immediately conclude from (2.89) and (2.92) that*

$$\tilde{p}_*^{(1)}(0)\ \cos\nu = \sqrt{\frac{\pi}{2\alpha}} - \sin\nu - \cos\nu = \sqrt{\frac{\pi}{2\alpha}} - \sqrt{2}\ \sin\frac{\pi^2}{8\alpha}. \tag{2.93}$$

Note that, for all cases $\alpha = \pi/(6+8k)$, where $k = 0, 1, 2, \ldots$ (that is, $m = 3 + 4k$ in terms of the discrete formulation), $\tilde{p}_*^{(1)}(0)$ takes its infinite value while the multiplication of (2.93) is always finite.

The only question that remains unanswered is the behaviour of the term $T(y)\cos\nu$ in (2.88) at zero and infinity, where the results of Appendix A are instrumental. Indeed, using the residuum theorem we conclude that for all cases, except the limiting one when $\alpha = \pi$, the following estimate is valid:

$$T(y) = \tilde{p}_*^{(1)}(0) - \frac{\pi y}{2} P_{-1} + \Gamma\left(1 - \frac{\pi}{\alpha}\right)\cos\frac{\pi^2}{2\alpha} P_*^- y^{\frac{\pi}{\alpha}} + O\big(y^2 \log y\big), \quad y \to 0, \tag{2.94}$$

where $\pi/\alpha > 1$. In the limiting case, $\alpha = \pi$, this estimate changes to

$$T(y) = \tilde{p}_*^{(1)}(0) - \frac{\pi y}{2}\big(Q_*^- + Q_{-1}\big(1 - \gamma - \log y\big)\big) + O\big(y^2 \log y\big), \quad y \to 0, \tag{2.95}$$

where $\gamma = -\Gamma'(1) \approx 0.5772156649$ is the Euler–Mascheroni constant see (for example Gradshteyn & Ryzhik (2014)).

To estimate the behaviour of the function $T(y)$ at infinity we note that the poles of the function $\tilde{p}_*^{(1)}(s)$ with positive real parts are simple and located at points $s_1^{(l)} = 2l + 1$, $l = 1, 2, \ldots$. On the other hand, the function $\cos(\pi s/2)$ has zeros at those poles. This might suggest an exponential decay for the function $T(y)$. However, there might also exist simple poles of the function $\tilde{p}_*^{(1)}(s)$ at points $s_2^{(l)} = 1 + \pi(1+2l)/(2\alpha)$, $l = 0, 1, \ldots$, and, consequently,

$$T(y) = \Gamma\left(1 + \frac{\pi}{2\alpha}\right)\sin\frac{\pi^2}{4\alpha} P_*^+ y^{-1-\pi/(2\alpha)} + O\big(y^{-1-3\pi/(2\alpha)}\big), \quad y \to \infty. \tag{2.96}$$

Thus, the decay is, generally speaking, not exponential. Note that the estimate (2.96) is the worst-case scenario. It does not contradict the known classic results (see Sretensky (1977) and Stoker (2019)), that, for $\alpha = \pi/(2m)$, the corresponding coefficients P_*^+ are zeros. See the discussions after (A6) in Appendix A.

https://doi.org/10.1017/jfm.2026.12121 Published online by Cambridge University Press

All constants in the asymptotic estimates (2.94)–(2.96) are defined in Appendix A. Moreover, $\tilde{p}_*^{(1)}(0)$ and P_{-1} and Q_{-1} are evaluated there explicitly, while P_*^-, Q_*^- and P_*^+ require computations of specific functionals acting on the solution of the integral equation.

Interestingly, taking estimate (2.94), Statements 2 and 3 and (A9) into account, the following immediately follows.

Statement 4. For arbitrarily $0 < \alpha < \pi$, there is an explicit relationship between the value of the potential $\phi(0, \pi)$ and its partial derivative over the boundary $\phi_r'(0, \pi)$ at the shoreline edge

$$\frac{\partial \phi}{\partial r}(0, \pi) = -2k\, e^{i\nu} \sqrt{\frac{\pi}{2\alpha}} \cot\alpha = -k\, \phi(0, \pi) \cot\alpha. \tag{2.97}$$

To the best of our knowledge, this result is new and might be important for the analysis of wave breakage near the shore edge.

Finally, when $\tilde{\phi}(s, \pi)$ has been found, we can also reconstruct the entire solution inside the water from (2.20)

$$\phi(r, \theta) = \frac{1}{2\pi i} \int_{-i\infty+\eta}^{i\infty+\eta} \frac{\Gamma(s)}{k^s} \frac{\cos s(\theta - \theta_0)}{\cos s(\pi - \theta_0)} \times \left((1+R)\left(1 + \tilde{p}_*^{(1)}(s)\right) \cos\frac{\pi s}{2} - (1-R) i \sin\frac{\pi s}{2} + i(1-R) \right) r^{-s} \mathrm{d}s. \tag{2.98}$$

Here, η can be taken equal to zero, while all functions decay exponentially along the imaginary axis. Moreover, a solution on the inclined boundary ($\theta = \theta_0$) can be written in the form

$$\phi(r, \theta_0) = \frac{1}{2\pi i} \int_{-i\infty+\eta}^{i\infty+\eta} \frac{\tilde{\phi}(s, \pi)}{\cos s\alpha} r^{-s} \mathrm{d}s = \frac{1}{\alpha} \int_0^\infty \frac{(rt)^{\frac{\pi}{2\alpha}}\, \phi(t, \pi)}{t^{\frac{\pi}{\alpha}} + r^{\frac{\pi}{\alpha}}} \frac{\mathrm{d}t}{t}, \tag{2.99}$$

since the solution on the surface of the free water has already been computed in (2.88). Note that $\phi(r, \theta_0) \to \phi(r, \pi)$ as $\theta_0 \to \pi$. Another trivial fact is $\phi(0, \theta_0) = \phi(0, \pi)$. For numerical computations of (2.99), the following identity can be useful:

$$\int_0^\infty \frac{(rt)^{\frac{\pi}{2\alpha}}\, f(t)}{t^{\frac{\pi}{\alpha}} + r^{\frac{\pi}{\alpha}}} \frac{\mathrm{d}t}{t} = \frac{\alpha f(0)}{1 + r^{\frac{\pi}{2\alpha}}} + \int_0^\infty \frac{(rt)^{\frac{\pi}{2\alpha}}}{t^{\frac{\pi}{\alpha}} + r^{\frac{\pi}{\alpha}}} \left(f(t) - \frac{f(0)}{1 + t^{\pi/\alpha}} \right) \frac{\mathrm{d}t}{t}. \tag{2.100}$$

3. Numerical results and discussions

3.1. *Numerical scheme to solve the integral equation (2.77)*

In our calculations, we replace the integral defined on the half-axis by the one on a finite domain $(\epsilon, 1/\epsilon)$. We use a logarithmic mesh and Simpson's composite quadrature rule (exploiting the smoothness of the solution). Near the point $r = 1$, we take into account that the integral is understood in terms of Cauchy singular integration. The asymptotic behaviour (2.80) discussed above can be used to control the accuracy of the computation.

As a result, we compute a solution of the respective integral equation as a function of the parameter d_1. The solution, generally speaking, has a singularity of this kind

https://doi.org/10.1017/jfm.2026.12121 Published online by Cambridge University Press

$$p_*^{(1)}(r, d_1) \sim \frac{\varpi(d_1)}{r-1} = \frac{\varpi_1 - d_1\varpi_d}{r-1}, \quad r \to 1, \tag{3.1}$$

that can be easily traced numerically. We optimise the solution with respect to the parameter d_1 to ensure its smoothness at point $r = 1$ by requiring the condition $\varpi(d_1) = 0$. Since $\varpi(d_1)$ is a linear function of the parameter d_1, one can use any method to compute its unique value ($d_1 = \varpi_1/\varpi_d$).

REMARK 9. *This analysis highlights why the parameter d_1 can have an infinite value despite condition (2.78). Namely, in such cases, a part of the solution of the integral equation corresponding to the right-hand side represented by the only function $n_d(r)$ is smooth at the point $r = 1$ (or equivalently, $\varpi_d = 0$). To avoid this inconvenience, we can search for a solution of the problem in the form (2.88) instead of (2.21). As a result, the respective equation to find d_1 would read $\varpi_1 \cos\nu + \varpi_d \sin\nu = 0$ (compared with (2.83)). However, we stay with our chosen approach for two reasons. First (see Remark 10), there are no problems in the computations related to such cases in practice. Second, we need to know from the beginning that $|R| = 1$ is to follow this route. In this paper, it is always the case (even though we started pretending not to know that and have proven this rigorously). However, in the cases where one searches for a singular solution to the problem Lewy (1946) and Sretensky (1977), this is not always true, and preserving the reflection coefficient R in the analysis instead of the phase shift ν is the only proper way to go. This will be the subject of another paper.*

3.2. *Comparison of the numerical solution with the exact one for discrete case: $\alpha = \pi/(2m)$*

Note that (2.77) can be solved analytically in the discrete case.

The case $\theta_0 = \pi + \pi/2$. We observe that $n_0(r, \theta_0) \equiv 0$ and thus the integral operator $\mathcal{N}$ vanishes. As a result, the unique solution of the integral equation is $q_*^{(1)} = 0$ and $d_1 = 0$. Due to (2.82), we conclude that $R = 1$, and the entire solution is represented by the function $U_0(r)$ describing waves at infinity, as expected.

The case $\theta_0 = \pi + \pi/4$. Now we can check that $n_0(r, \theta_0) = -n_d(r, \theta_0)$. Thus, the only solution from the required class is $d_1 = -1$, $p_*^{(1)}(r) = 0$ and $R = i$ (compare with (2.82)) or the phase shift, $\nu = \pi/4$, (2.83). This result naturally coincides with the well-known one from Lewy (1946), Stoker (1947) and Sretensky (1977).

The case $\theta_0 = \pi + \pi/(2m)$. For those cases $n_0(r, \theta_0)$ and $n_d(r, \theta_0)$ are no longer linearly dependent. However, if one specifies the representation (2.60) even further (using the arguments $\pi s/(2m)$, $m = 2, 3, 4 \ldots M$ in the trigonometric functions), the respective function n_d will change and the solution of the equation can still be computed in a close form, while the solution will be the same cumbersome as in the classic case (compare with Lewy (1946)). Those solutions will decay exponentially at infinity and the respective phase shift is equal to $\nu = \pi(m-1)/4$, as expected (Lewy 1946; Stoker 1947). We do not go in this direction; simply compute the integral equation for some of the discrete angles $\theta_0 = \pi + \pi/(2m)$.

We start with the verification of our integral equation (2.77) (and the entire solution) comparing it with the discrete cases $\alpha = \pi/(2m)$, $m = 1, 2, \ldots$. Note that the solution of the integral equation for the cases $m = 1, 2$ should be, as discussed above, identically zero. In fact, the respective curves in figure 2(*a*) lie below the threshold of 10^{-15}, which is the precision of the MATLAB calculations. Note that the spikes observed in the curves plotted in log–log scale correspond to the zeros of the solution of the integral equation, that is, to the points where these real functions change sign.

https://doi.org/10.1017/jfm.2026.12121 Published online by Cambridge University Press

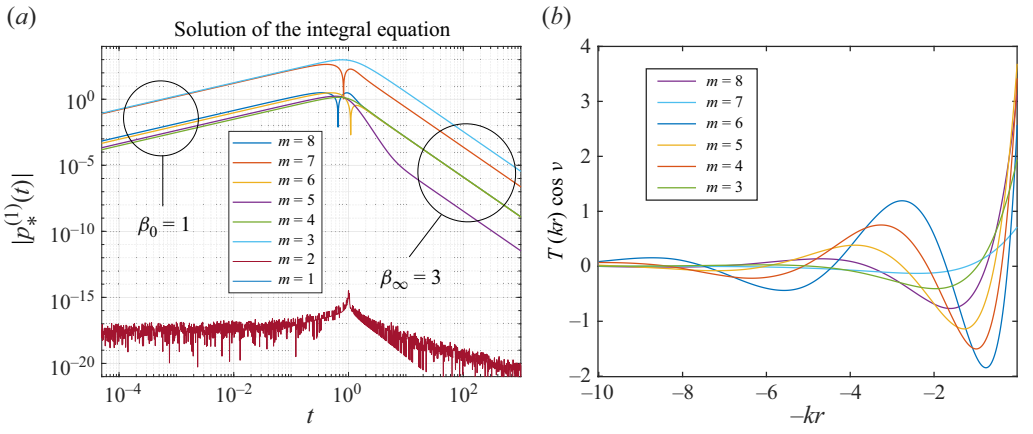


Figure 2. (*a*) Absolute value of the (real) solutions $p_*^{(1)}(t)$ of the integral equation (2.77) for different angles $\alpha = \theta_0 - \pi = \pi/(2m)$, $m = 1, 2, \ldots, 8$. The graphs are presented in log–log scale thus the spikes inside the interval correspond to zero values of the solutions. (*b*) Shows the respective inversion of the second term in the representation (2.88). Note that the curves for $m = 1, 2$ are identically zero, while those for $m = 3, 7$ are close to zero due to the extremely small value of the multiplier, $\cos\nu$.

The remaining six curves behave as expected in the estimate (2.80) with the exponents $\beta_0 = 1$ and $\beta_\infty = 3$. Those facts are consistent with the analysis provided in Appendix A (compare with discussion around (A5)).

Note that the values of the solution of the integral equation, $p_*^{(1)}(t)$, for $m = 3, 7$ are a few orders of magnitude higher than for the other cases (compare with figure 2(*a*)). In fact, if one reformulates the problem with new unknown functions $\tilde{p}_*^{(j)}(s)\cos\nu$ instead of $\tilde{p}_*^{(j)}(s)$, it would work for all cases.

To make this point exposed, in figure 2(*b*) we presented the inverted terms in the representation (2.88). It represents the main part of the localised part of the solution. Evanescent waves are drawn in figure 4(*a*), while the entire water surface profile is given in figure 4(*b*).

Having the function $p_*^{(1)}(t)$ at hand, we can compute the value $\phi(0, \pi)$ from (2.88) and thus verify the identity (2.92), which has been proved valid for any discrete solution. Note that the values of the reflection coefficients R are computed from the formula (2.82) when solving the integral equation (see the discussion around (3.1). The respective results are presented in figures 3(*a*) and 3(*b*).

REMARK 10. *We would like to highlight the case* $R = -1$ *(which corresponds to* $\cos\nu = 0$ *and thus to* $d_1 = \infty$*). This solution should formally fail in our computations. However, since all integrals are computed with some accuracy, the constant* d_1 *appears in the computations as a large number, but it is still finite. As a result, the respective solution coincides with the analytical one for* $\alpha = \pi/(2m)$, $m = 3, 7$*) within the range of accepted accuracy level.*

We observe that as the angle decreases, the computational challenges increase. This has been predicted (see discussions around (2.78)). It is clear that, by increasing the number of mesh points, we could improve the accuracy if needed. However, for extremely small angles α, the shallow-water approximation should be used naturally instead. Moreover, the sensitivity of the reflection coefficient becomes an issue and should be questioned against the physical phenomena behind the potential flow.

https://doi.org/10.1017/jfm.2026.12121 Published online by Cambridge University Press

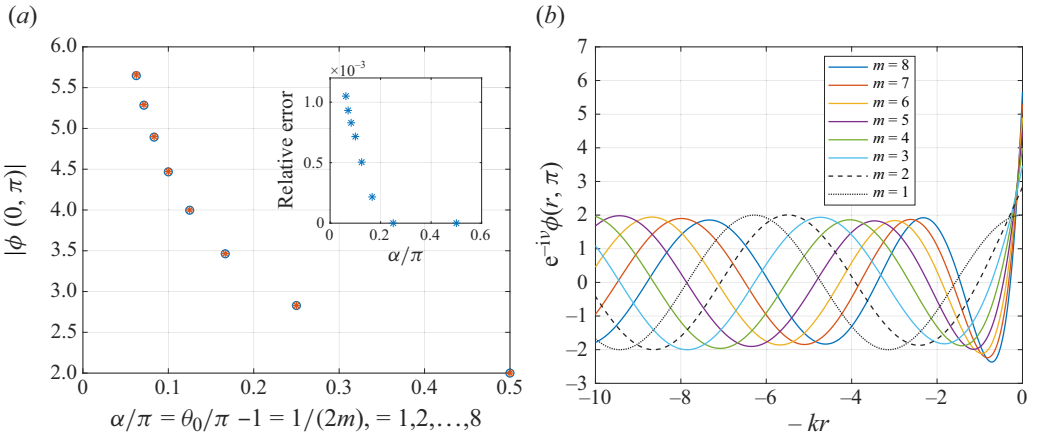


Figure 3. Indirect verification of the computational accuracy of the integral equation (2.77) for different angles $\alpha = \theta_0 - \pi = \pi/(2m)$, $m = 1, 2, \ldots, 8$ by comparing the numerical and exact analytical values of the reflection coefficient and the value of the potential at zero point along the water surface ($z = 0$).

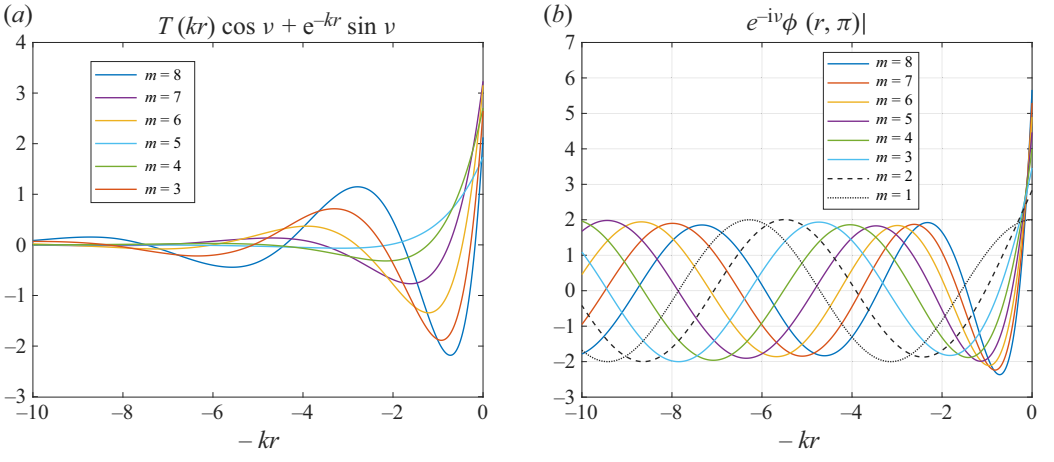


Figure 4. (*a*) Evanescent waves along the water surface for different angles $\alpha = \theta_0 - \pi = \pi/(2m)$, $m = 1, 2, \ldots, 8$. (*b*) Shows the full water surface. In case $m = 1, 2$, the solution is given analytically (respective curves are given by dashed and dotted lines.

In figure 4(*a*) we present the localised part (evanescent waves), while in figure 4(*b*) we show the entire profile of water surface ($z = 0$) for those values of the angle $\alpha = \pi/(2m)$, $m = 1, 2, \ldots$. In conclusion of this subsection, we confirm that the new method produces the same results as known from Lewy (1946), Stoker (1947) and Sretensky (1977). Note that these cases correspond only to the reflection coefficients $R = \pm 1, \pm i$.

3.3. *Verification of the Statements 2–3 for arbitrary angles* $0 < \alpha \leqslant \pi/2$

In this section, we compute the solution in the same region $0 < \alpha < \pi/2$. In our computations, we can take an arbitrary number. On the other hand, any angle can always be represented with an arbitrary accuracy in the form $\alpha = \pi p/(2m)$ and $p < 2m$ where the theory is available, but the respective analytical solution takes too complicated form

https://doi.org/10.1017/jfm.2026.12121 Published online by Cambridge University Press

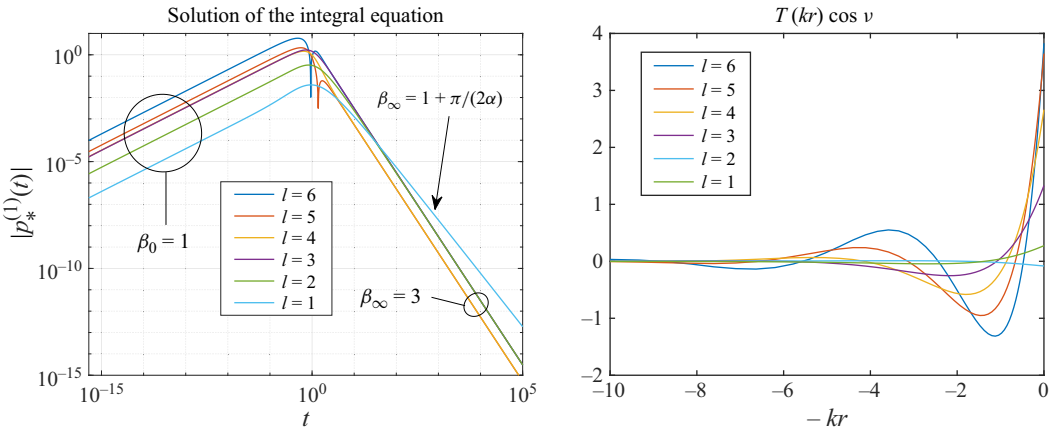


Figure 5. (*a*) Absolute value of the solutions $p_*^{(1)}(t)$ of the integral equation (2.77) for different angles $\alpha = \theta_0 - \pi = \pi/(2l+1)$, $l = 1, 2, \ldots, 6$. The graphs are presented in log–log scale thus the spikes inside the interval correspond to zero values of the solutions. Note that the value of the exponent $\beta_0 = 1$ for all cases. Differently for the exponent defining decay at infinity. Here $\beta_\infty = 3$ for all cases except $l = 1$ where $\beta_\infty = 1 + \pi/(2\alpha) = 5/2 < 3$ (see for details in Appendix A). An arrow depicts this respective curve. (*b*) Shows the respective inversion of the second term in the representation (2.88).

Lewy (1946), Stoker (1947) and Sretensky (1977). By the continuity argument, the global parameters of the solution as the phase shift (reflection coefficient) and the run-up ratio should be the same for angles $\alpha < \pi/2$. We verify below the Statements 2 and 3 for $\alpha = \pi/(2l+1)$, $l = 1, 2, \ldots$.

In figure 5(*a*) we present the absolute value of the numerical solutions of the integral equation (2.77) on the log–log scale. The only essential change compared with the results of the previous subsection (figure 2*a*) is the fact that for $\alpha = \pi/3$, the behaviour at infinity from the estimate (2.80) changes from $\beta_\infty = 3$ to $\beta_\infty = 1 + \pi/(2\alpha) = 3/2 < 3$. Such an effect has been predicted in the more detailed analysis of the solution given in Appendix A. It was not previously observed for the angles $\alpha = \pi/(2m)$, and the values $\alpha = \pi/4$ and $\pi/2$ led to a trivial solution of the integral equation. We also note that in the cases under consideration all solutions have maximal values of the order of 10^0 instead of 10^3 as previously for those cases $m = 3, 7$ where d_1 were large.

In figure 5(*b*), as previously, we present the second term in the representation (2.88) for different values of the angle α. Now the multiplier $\cos\nu$ plays no role in the calculations as it always takes the same absolute value $1/\sqrt{2}$.

In figures 6(*a*) and 6(*b*) we verify the formulas of Statements 2 and 3. The accuracy is on the same level (or better) as in the previous subsection. Finally, in figures 7(*a*) and 7(*b*), we present the evanescent waves and the full profile of the potential along the water surface ($z = 0$).

Thus, we can confidently conclude that Statements 2 and 3 are valid for the angles $0 < \alpha \leqslant \pi/2$. The deviations of the numerically computed values from the analytical formulas are due to the numerical error. The latter increases for smaller angles of α as we have already discussed in the previous subsection.

In the next subsection, we will analyse the formulas (2.92) and (2.91) from Statements 2 and 3 that represent the phase shift and the run-up for the values of α from the interval $\pi/2 < \alpha \leqslant \pi$. We use the same numerical scheme to solve the integral equation (2.77).

https://doi.org/10.1017/jfm.2026.12121 Published online by Cambridge University Press

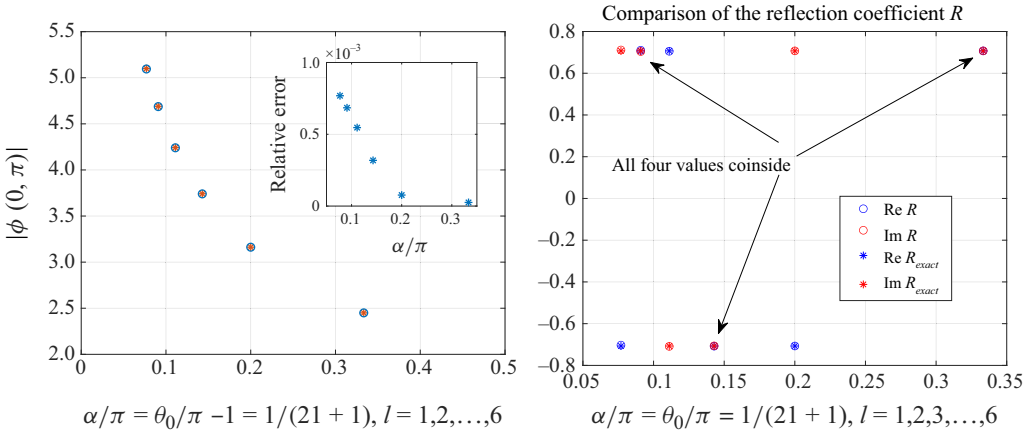


Figure 6. Verification of the Statements 2 and 3 for different angles $\alpha = \theta_0 - \pi = \pi/(2l+1)$, $l = 1, 2, \ldots, 6$ by comparing the numerical and the predicted analytical results.

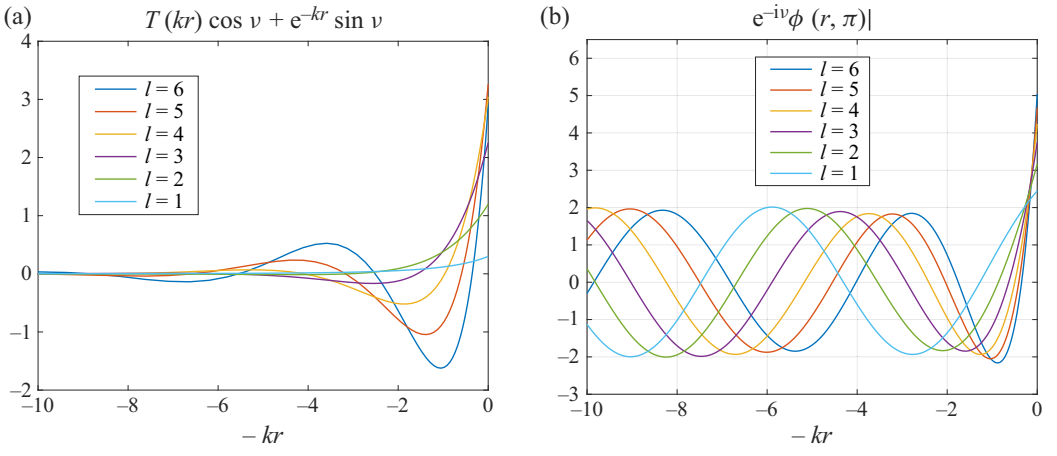


Figure 7. (*a*) Evanescent waves along the water surface for different angles $\alpha = \theta_0 - \pi = \pi/(2l+1)$, $l = 1, 2, \ldots, 6$. (*b*) Shows the full water surface.

3.4. *Verification of the Statements 2–3 for arbitrary angles* $\pi/2 < \alpha \leqslant \pi$

In figure 8(*a*), we show the respective solutions of the integral equations for a few values of $(\alpha/\pi = 0.51, 0.6, 0.7, 0.8, 0.9, 1.0)$. As seen, now the exponent, $\beta_\infty = \beta_\infty(\alpha)$ in the asymptotics at infinity (2.80) depends on the angle α, while $\beta_0 = 1$ remains. Only in the limiting case ($\alpha = \pi$), the leading term in the asymptotics $(2.80)_1$ changes to $t \log t$ as predicted in Appendix A. This fact is hardly visible, so we indicate it by an arrow.

The second term in the solution representation (2.88) now changes its behaviour. It no longer indicates the oscillatory character in contrast to the case $0 < \alpha < \pi/2$. Also, the values are an order of magnitude smaller than in the case $0 < \alpha < \pi/2$ while the decay is different (no longer exponential).

In figures 9(*a*) and 9(*b*), we verify the formulas for the reflection coefficient and the run-up from Statements 2 and 3 for different angles α as shown in the legend. For the same numerical settings, the computational accuracy is higher than for smaller angles $\alpha \in (0, \pi/2)$. Moreover, the variation of the reflection coefficient is much slower now

https://doi.org/10.1017/jfm.2026.12121 Published online by Cambridge University Press

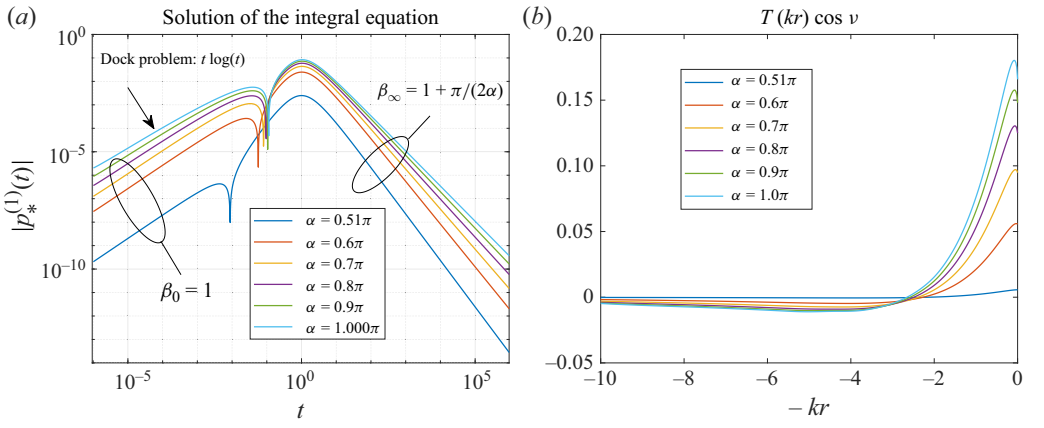


Figure 8. (*a*) Represents the absolute value of the solutions $p_*^{(1)}(t)$ of the integral equation (2.77) for different angles $\alpha = \theta_0 - \pi$ as indicated in the legend. The graphs are presented in log–log scale thus the spikes inside the interval correspond to zero values of the solutions. The value of the exponent $\beta_0 = 1$ for all cases except for $\alpha = \pi$ when the asymptotic is different (it contains also a logarithmic term). As for the other exponent, β_∞, it now depends on the angle $\beta_\infty = 1 + \pi/(2\alpha) \in (3/2, 2) < 3$ (see for details in Appendix A). (*b*) Shows the respective inversion of the second term in the representation (2.88).

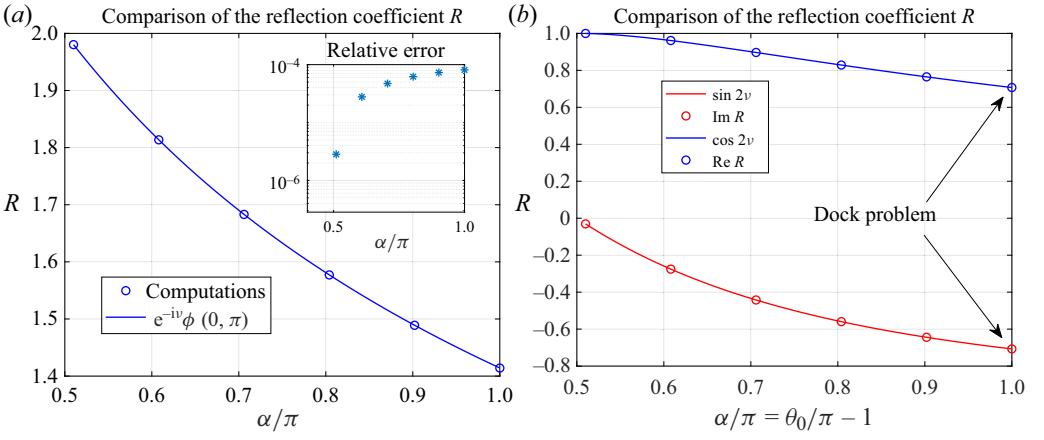


Figure 9. Verification of the formulas for the run-up and the reflection coefficient as shown in the legend from Statements 2 and 3 for different angles $\alpha > \pi/2$. For the same numerical settings, the computational accuracy is higher than for smaller angles $\alpha < \pi/2$.

(no oscillations at all). In the limiting case ($\alpha = \pi$) the values coincide with those of the dock solution (Chakrabarti *et al.* 2005).

To conclude analysis of this case, we present in figures 10(*a*) and 10(*b*), the entire localised part of the solution near the full water profile along the water surface, respectively. As mentioned above, the localised part is much less pronounced for $\pi/2 < \alpha \leqslant \pi$ than in the case of smaller angles, that is, $0 < \alpha < \pi/2$.

To summarise the verification from Statements 2 and 3 in the entire range of the beach slope $0 < \alpha \leqslant \pi$, in figure 11, we present analytical and numerical results for the reflection coefficient and the run-up at the beach edge.

https://doi.org/10.1017/jfm.2026.12121 Published online by Cambridge University Press

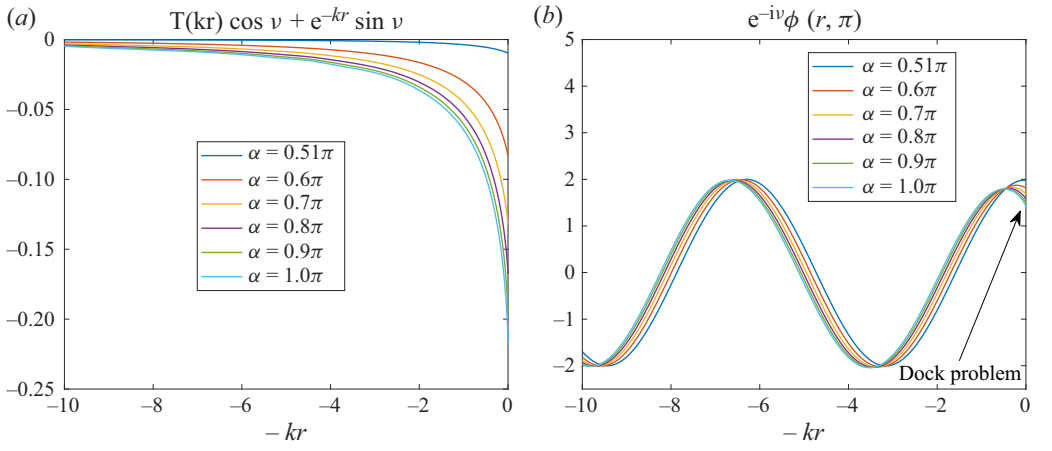


Figure 10. (*a*) Localised part of the solutions along the water surface for different angles α as indicated in the legend, while (*b*) shows the full profile of potential at $z = 0$.

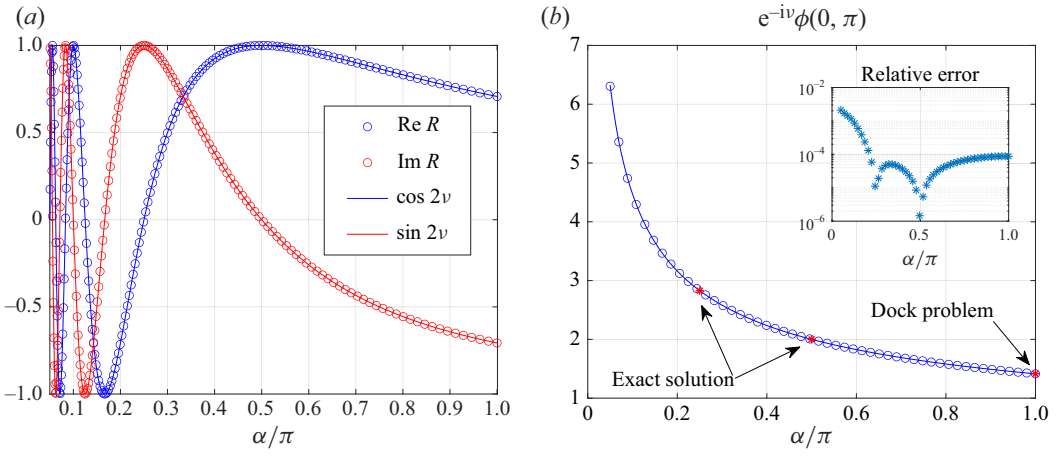


Figure 11. Summary on the validity of the formulas from Statements 2 and 3 in the entire domain of the angle $0 < \alpha \leqslant \pi$. All available results have been used for the verification. Accuracy of the computations for the fixed set of technical parameters when computing the solution $p_*^{(1)}(t)$ of the integral equation and evaluating the function $T(y)$.

3.5. *Computation of pressure on the seabed for various beach angles* $0 < \alpha \leqslant \pi$

In this subsection, we analyse the impact of water waves on the seabed, with the pressure computed as $p(r, t) = p_0 + \rho g r \sin\alpha + \mathrm{Re}\{i\rho\omega\phi(r, \theta_0)e^{-i\omega t}\}$ or

$$p(r, t) = p_0 + \rho g r \sin\alpha + \rho\omega \cos\left(\frac{\pi}{2} + \nu - \omega t\right) e^{-i\nu}\phi(r, \theta_0). \tag{3.2}$$

In figure 12(*b*), we present the distribution of the normalised potential $e^{-i\nu}\phi(r, \theta_0)$ along the water bed ($\theta = \theta_0 = \alpha + \pi$) for various angles α smaller than $\pi/2$ (figure 12*a*) and larger than $\pi/2$ (in figure 12(*b*)). It preserves the same features in terms of monotonicity as the free water surface.

https://doi.org/10.1017/jfm.2026.12121 Published online by Cambridge University Press

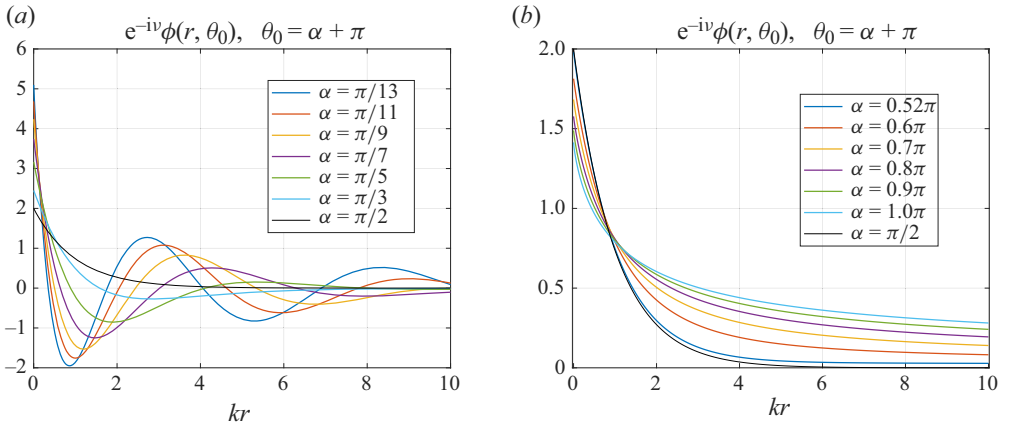


Figure 12. The figure presents the normalised potential along the water bed ($\theta=\theta_0=\alpha+\pi$) for various angles α smaller than $\pi/2$ (a) and larger than $\pi/2$ ((b)).

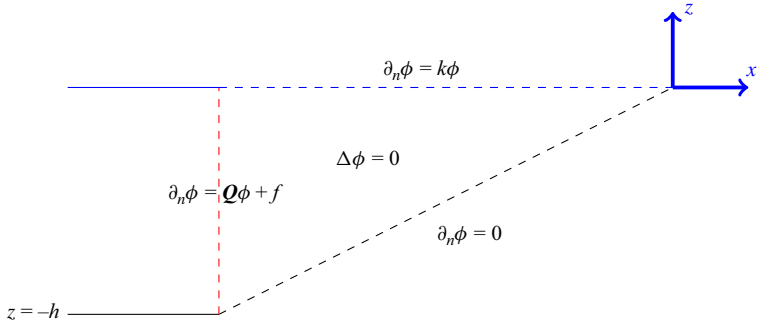


Figure 13. Geometric setting used for the BEM computations. The boundaries are the dashed lines with the normal derivative given by the equations shown.

3.6. *Numerical validation using the boundary element method*

Although we have strong evidence of the accuracy of our results, we also validated them using the BEM. This allowed us to check the reflection coefficient and the free surface displacement. The BEM is a numerical method that is ideally suited to solving the Laplace equation. For our problem, we use a modification of the method outlined in Wang & Meylan (2002). Note that the BEM code can be downloaded from WikiWaves (2010). Figure 13 shows the finite triangular region used to approximate the solution with the boundary conditions. All details can be found in Wang & Meylan (2002). Note that the left-hand boundary condition is not pointwise because it involves a linear operator $\mathbf{Q}$. For our calculations, we assume $k=1$ and the depth (of the computational domain) is $h=4$.

The BEM that we use has linear elements and the convergence will be linear with the size of the panel. We consider two panel sizes, approximately 0.025 and 0.0125 (note that these are by necessity approximate since the lengths of each sides will not necessarily be divisible by the panel size). Figure 14 shows the exact and BEM solution for the reflection coefficient, R, as a function of α and ν. As expected, the error increases as the angle decreases and behaves approximately as $1/\alpha$ for small values of α. Note that the same panel size is used here, so that as the angle increases, the size of the BEM matrices increases significantly. Figure 15 shows the solution for the two panel lengths. On the

https://doi.org/10.1017/jfm.2026.12121 Published online by Cambridge University Press

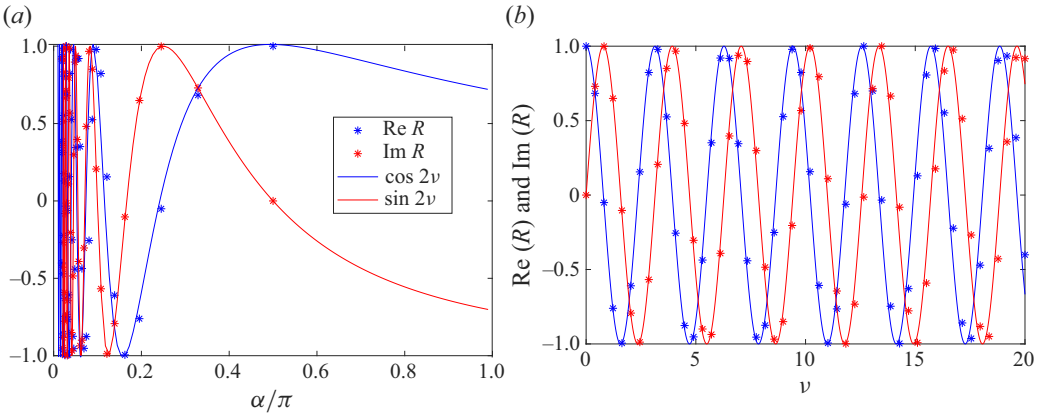


Figure 14. Real and imaginary part of R as a function of α/π (a) and ν (b). The solid line is the exact solution and the dots are the solution by the BEM, with panel size approximately 0.025.

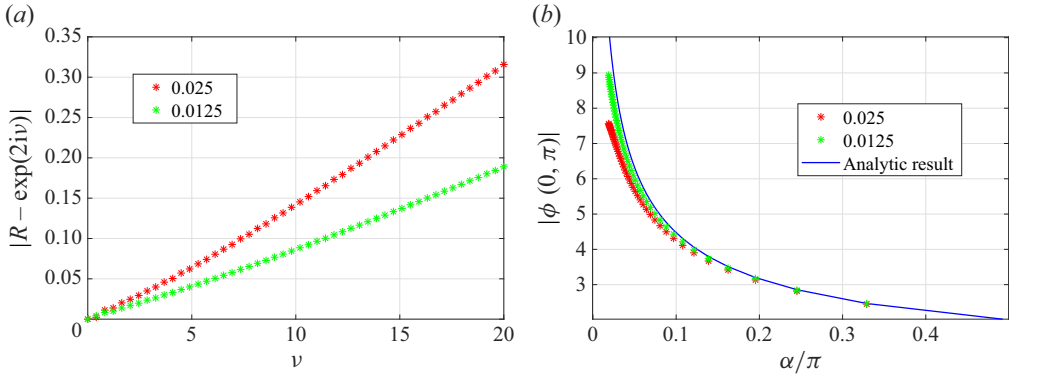


Figure 15. The absolute value of the difference between the reflection coefficient, $|R|$, calculated by the BEM and the exact solution (a) and the absolute value of the potential at the end, $|\phi(0,\pi)|$, calculated using the BEM and the exact formula (b). Note that the step sizes are approximately 0.025 (red) and 0.0125 (green).

left, we show the error of the reflection coefficient and, on the right, the solution for the displacement at the end. Note that the end displacement is calculated using a linear extrapolation of the second and third last elements because there are large errors for the final element. Linear convergence with panel size is apparent, as is the linear growth in error with respect to ν (we note that this linear growth with ν does not follow from the linearity of the elements).

Finally, we note that the BEM is a numerical method with great flexibility, for example, it can be extended to non-uniform beach profiles, obstacles etc. For more complicated problems, for example, where there is a singularity at the end point, and for which no analytic results exist, the BEM would provide a useful validation.

4. Solution in time domain

We present here the solution in the time domain. We note that in Meylan (2009) a very general theory for the time-dependent problem was presented for an arbitrary seabed. In

https://doi.org/10.1017/jfm.2026.12121 Published online by Cambridge University Press

particularly, the following identity was proven:

$$\int_{-\infty}^{0} \phi(r,\pi,k)\overline{\phi(r,\pi,k')}\mathrm{d}x = 2\pi\delta(k-k'), \tag{4.1}$$

where the overline denotes complex conjugate. Note that this formula is the same as (2.5) of Ehrenmark & Body (2001) who proved it for the case of a straight-line beach as we consider here. A similar formula for only certain angles was given in Dorfman (1984). This result was shown to be true for very general bottom surfaces by Meylan (2009).

As a result, if we only want to calculate the displacement $\zeta(r,t)$ and the initial surface displacement is $\zeta(r,0)=\zeta_0$ and the initial surface velocity is zero, i.e. $\partial_t\zeta_0(r,0)=0$, the following relationship provides the displacement:

$$\zeta(r,t) = \frac{1}{2\pi}\int_0^{\infty} \langle\zeta_0(r),\phi(r,\pi,k)\rangle\phi(r,\pi,k)\cos(\omega t)\mathrm{d}k, \tag{4.2}$$

where $\omega=\sqrt{gk}$, while the inner product is given by

$$\langle\zeta_1,\zeta_2\rangle = \int_{-\infty}^{0}\zeta_1(r)\overline{\zeta_2(r)}\,\mathrm{d}x. \tag{4.3}$$

4.1. *Numerical calculation*

Solving (4.2) numerically can be accomplished straightforwardly by converting to matrix multiplication as outlined in Wilks *et al.* (2024, 2025). We divide r and k into a set of even points r_i and k_j with spacing Δr and Δk respectively. For our numerical calculations, we choose 1000 points for x from -20 to 0 and for k we choose 5000 points between 0 and 5. We define the matrix

$$\mathbf{P}=[P_{ij}],\ P_{ij}=\phi(r_i,\pi,k_j). \tag{4.4}$$

Then

$$\mathrm{vector}[\zeta(r_i,t+t_0)] \approx \frac{\Delta r\Delta k}{2\pi}\mathbf{P}\times\mathrm{diag}[\cos(\omega_j t)]\times\mathbf{P}^{\star}\times\mathrm{vector}[\zeta(r_i,t_0)], \tag{4.5}$$

where vector means to convert the sequence of points to a column vector and diag denotes the same conversion to a diagonal matrix. The star denotes the complex conjugate transpose. We note that we only need to calculate the matrix $\mathbf{P}$ once and can then solve for any initial condition and at any time. Except for the fact that we do not consider the initial value of the time derivative (which is only to keep the explanation simple), we have effectively calculated the operator $\exp(-\mathrm{i}\mathcal{P}t)$ and expressed it as matrix multiplication.

We also note that we could choose the number of points in r and k to be the same, say, N and the spacings Δr and Δk in such a way that

$$\frac{\Delta r\Delta k}{2\pi} = \frac{1}{N}. \tag{4.6}$$

This would in some sense be the optimal choice, and we note that this is what is done when converting the Fourier transform to the fast Fourier (or discrete) Fourier transform in the standard implementations. Further details of this can be found in Wilks *et al.* (2024, 2025).

We present some time-domain results with a solution with an initial condition

$$\zeta_0 = 2e^{-(x+3)^2},\quad x\le 0,\quad (r=-x,\quad \theta=\pi). \tag{4.7}$$

Figure 16 shows the evolution of the fluid surface for the initial condition given by (4.7) with no initial velocity. The slopes are $\alpha=0.089\pi, 0.186\pi$ and 0.380π.

https://doi.org/10.1017/jfm.2026.12121 Published online by Cambridge University Press

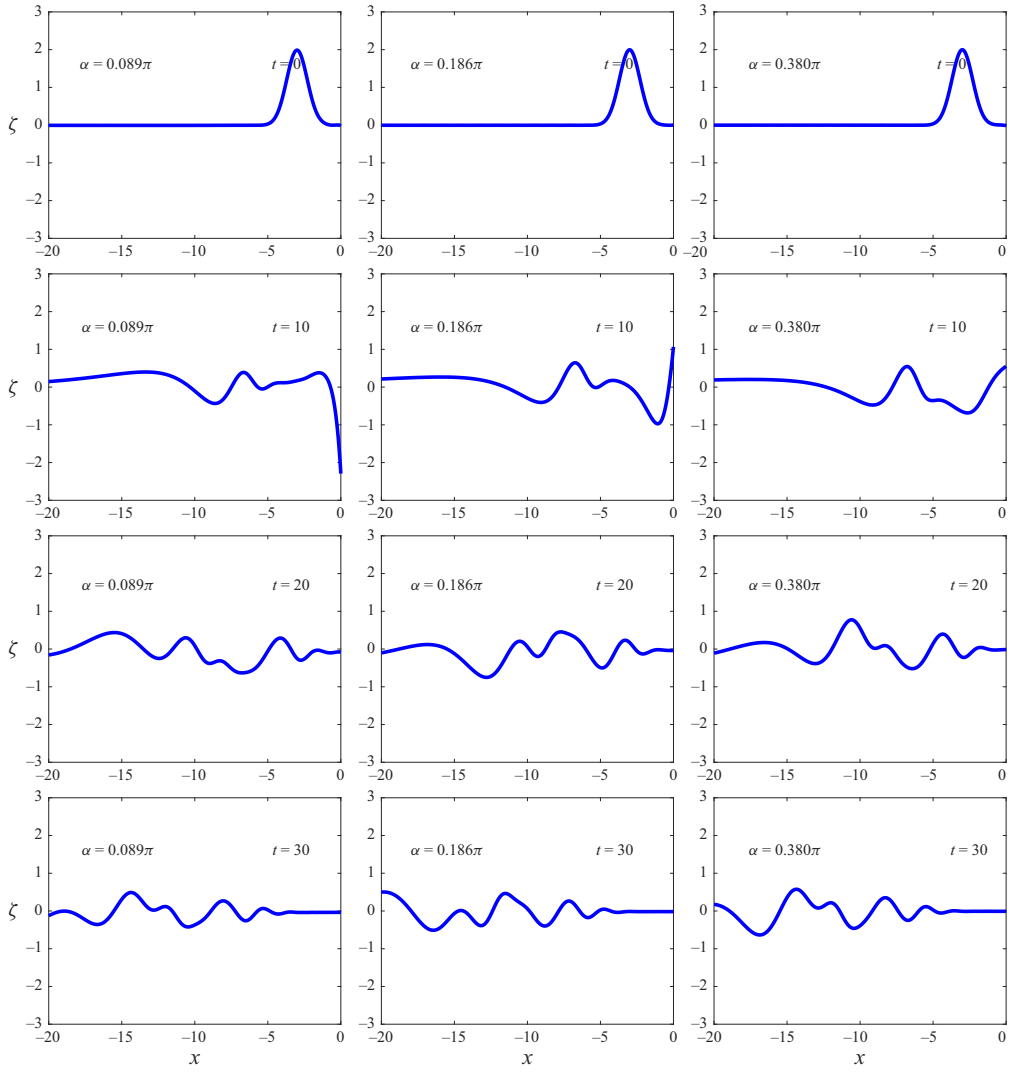


Figure 16. The evolution of the fluid surface for the initial condition given by (4.7) with no initial velocity. The slopes are $\alpha = 0.089\pi, 0.186\pi$ and 0.380π. The non-dimensional times (gravity is assumed unity) are shown. The animations can be found in the supplementary material (Movies 1–3), available at https://doi.org/10.1017/jfm.2026.12121.

The non-dimensional times (gravity is assumed unity) are shown. The animation can be found in the supplementary material as Movies 1–3. Figure 16 shows the evolution of the slopes $\alpha = 0.089\pi$, 0.186π and 0.380π, respectively. Figure 17 is the same as figure 16 except for $\alpha = 0.477\pi$, 0.670π and 0.864π. The animation for this figure can be found in the supplementary material as Movies 4–6. Note that the solution for these and subsequent figures is given for non-dimensional time (assuming gravity is unity). The pulse initially travels in both directions and the right-travelling wave leads to a high amplitude on the beach before being reflected. As the angle of the beach increases the run-up decreases, and also the figures become more and more similar, reflecting the fact that the variation in the frequency-domain solutions becomes less as the angle increases.

https://doi.org/10.1017/jfm.2026.12121 Published online by Cambridge University Press

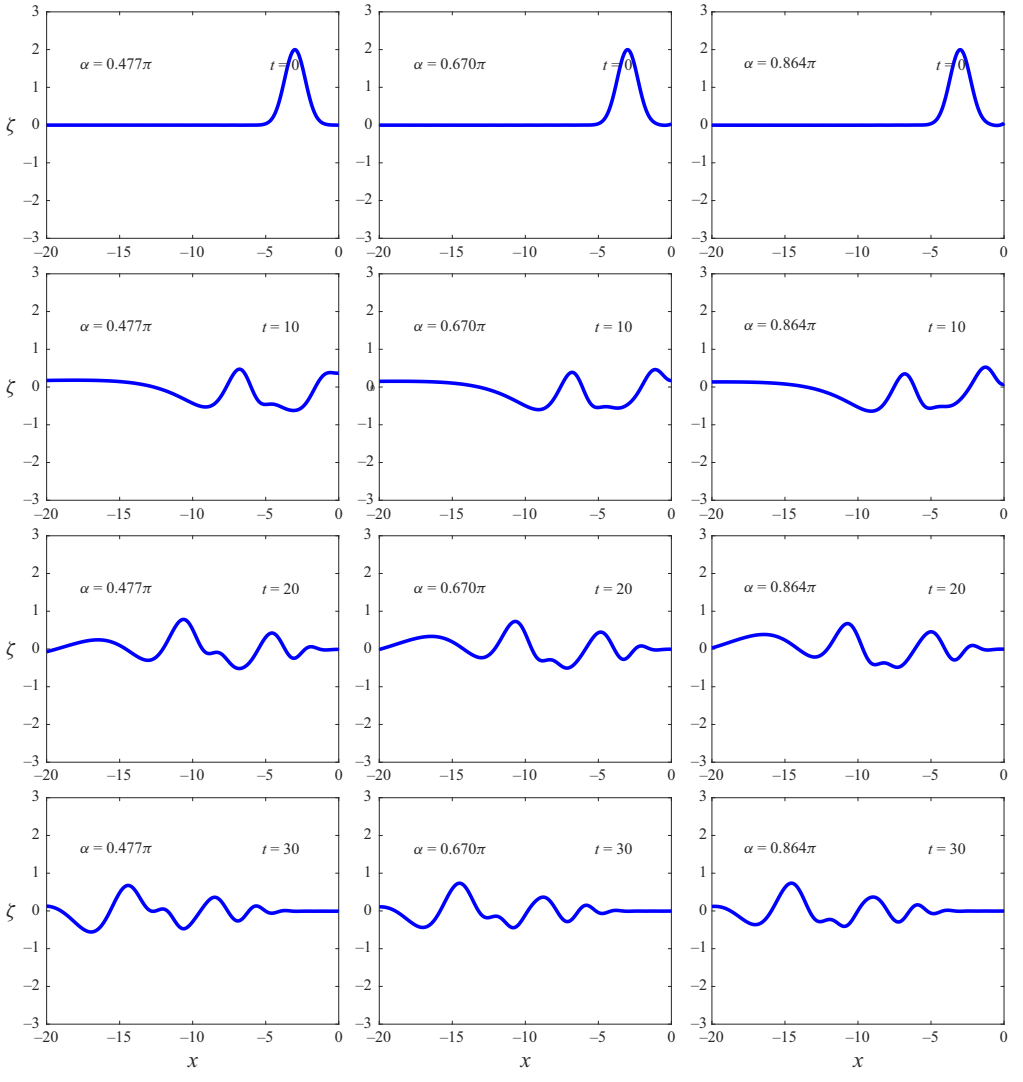


Figure 17. As in figure 16 except $\alpha = 0.477\pi$, 0.670π and 0.864π. The animations can be found in the supplementary material as Movies 4–6.

4.2. *Solution for an incident wave packet*

The formulation given expresses the solution as a weighted integral of the frequency-domain solutions, where the weighting is calculated using an inner product. A simpler approach is to impose the weighting and express the solution as

$$\zeta(r, t) = \mathrm{Re}\left\{\int_0^\infty \hat{f}(k)\phi(r, \pi, k)\exp(-\mathrm{i}\omega t)\mathrm{d}k\right\}, \tag{4.8}$$

where we specify $\hat{f}(k)$. For the numerical examples, we choose

$$\hat{f}(k) = \sqrt{\frac{5}{\pi}}\exp\left(-5(k-2)^2\right). \tag{4.9}$$

https://doi.org/10.1017/jfm.2026.12121 Published online by Cambridge University Press

Note that this calculation can be transformed to a matrix multiplication, as outlined in the previous section. This is not an initial value problem. The wave packet is incident from negative infinity and $t = 0$ is set to be the time the centre of the pulse would reach $r = 0$ if the depth remained infinite. Therefore, we can consider negative time.

Figure 18 shows the evolution of the wave packet given by (4.9) for the non-dimensional times (gravity is unity) shown with slopes $\alpha = 0.089\pi$, 0.186π and 0.380π. The animation can be found in the supplementary material as Movies 7–9. Figure 19 is the same as figure 18 except for $\alpha = 0.477\pi$, 0.670π and 0.864π. The animation for this figure can be found in the supplementary material as Movies 10–12. As shown in figures 16 and 17 the variation in solution is less as the angle increases. The amplification of the pulse at the beach end is clearly apparent for small angle α.

Finally, we compute the wave height on the shoreline $\zeta(t, 0)$ divided by $\tan^2(\alpha)$ for the initial pulse (figure 20*a*) and the incident pulse (figure 20*b*). The values for all parameters are the same as in figures 16 and 18. The normalisation of this kind has been chosen to make both results equally visible. It was suggested by Miche's wave breakage condition (Miche 1944) that states wave breaking occurs when the slope of the seabed, S, becomes smaller than the gradient of the wave-induced surface elevation, $\max_t \zeta'_x(t, 0) > S = \tan\alpha$, where $\zeta(t, x)$ is the elevation of the water surface, computed from (4.2) for the initial pulse and from (4.8) for the incident packet. For monochromatic waves, Miche's criterion in our notation (compare with (2.97)) reads: $\max_t \zeta(t, 0) > k^{-1}\tan^2\alpha$. The mixture of frequencies in these two cases is very different, but the scaled amplitude on the beach in both cases is similar. Since the initial pulse breaks into two waves which travel in opposite directions, in some sense both waves have non-dimensional amplitude unity near the beach.

5. Conclusions

In this study, we have revisited the classical problem of wave propagation on a sloping beach of arbitrary inclination and developed a unified framework for the computation of regular solutions valid for any angle $0 < \alpha \leqslant \pi$. Using the Mellin-transform technique, the governing equations were reduced to a system of singular integral equations on the half-axis, characterised by fixed-point singularities at zero point, an internal point and at infinity. The proposed approach has been shown to be highly efficient across the entire range of beach slopes, ensuring a smooth transition between known results. In particular, it enabled the derivation of exact expressions for the reflection coefficient, phase shift and the shoreline run-up, previously proven for acute angles. We also evaluated a new exact relationship between the run-up and the profile gradient at the shoreline, providing further physical insight into nearshore wave behaviour.

The frequency-domain solutions were further employed to construct time-dependent solutions through a matrix representation that generalises the diagonalisation of self-adjoint operators, following recent theoretical advances in matrix factorisation. The resulting formulation offers a computationally effective means of evaluating transient wave fields and compares favourably with known results from the literature.

While the present analysis focuses on regular water wave solutions, the proposed framework is sufficiently flexible to accommodate extensions to other solution classes, including cases involving singular behaviour, which will be explored in future work.

https://doi.org/10.1017/jfm.2026.12121 Published online by Cambridge University Press

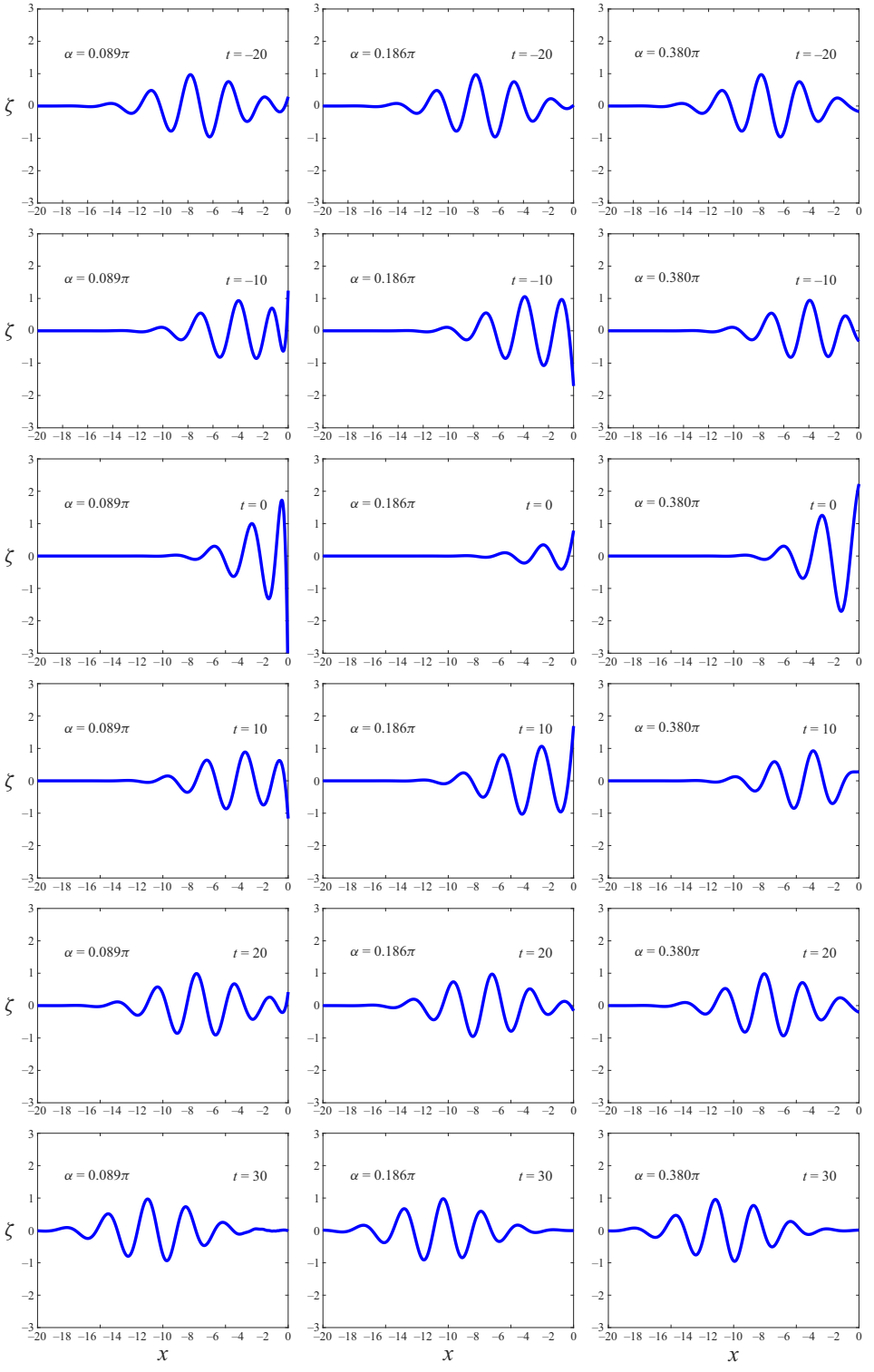


Figure 18. The evolution of the wave packet given by (4.9) for the non-dimensional times (gravity is unity) shown with slopes $\alpha = 0.089\pi, 0.186\pi$ and 0.380π. The animations can be found in the supplementary material as Movies 7–9.

https://doi.org/10.1017/jfm.2026.12121 Published online by Cambridge University Press

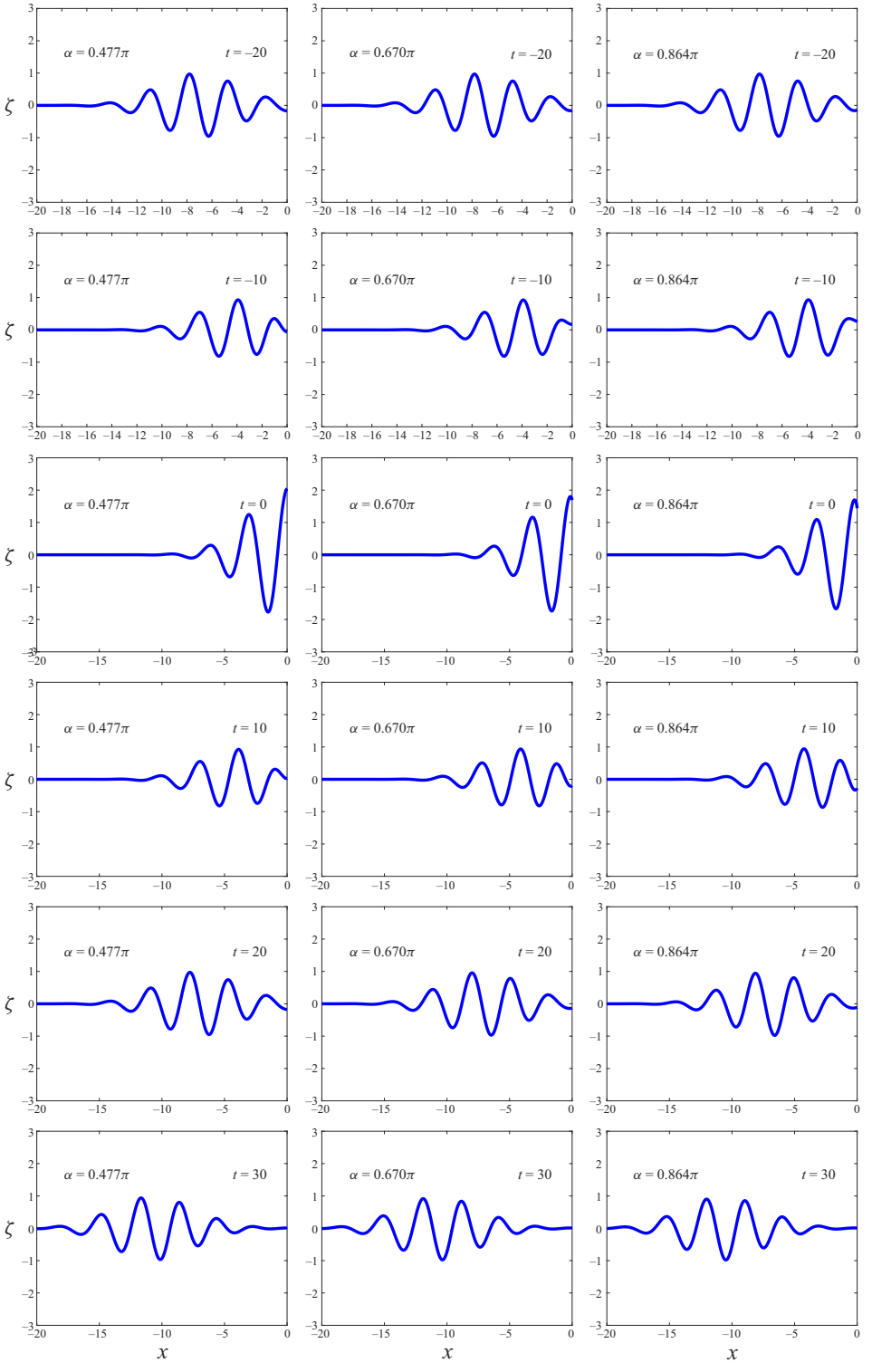


Figure 19. As in figure 18 except $\alpha = 0.477\pi$, 0.670π and 0.864π. The animations can be found in the supplementary material as Movies 10–12.

https://doi.org/10.1017/jfm.2026.12121 Published online by Cambridge University Press

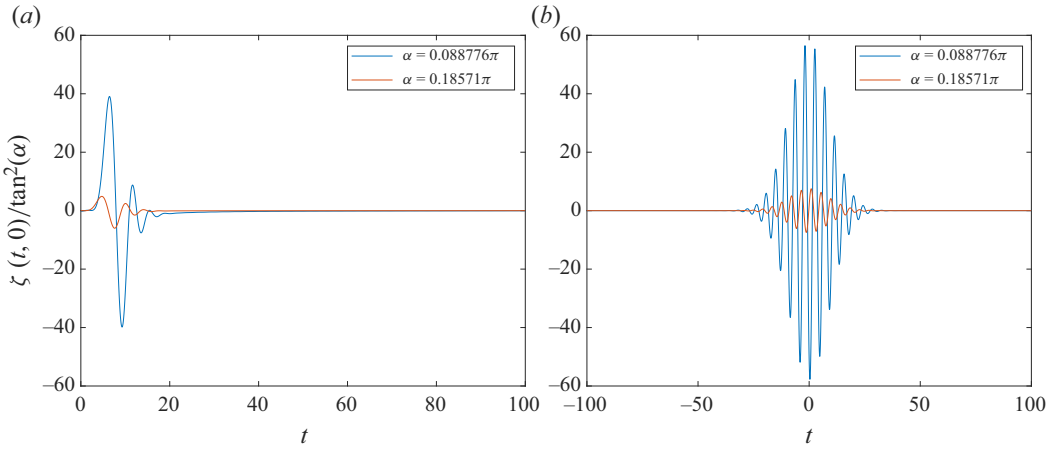


Figure 20. The height of the wave at the shoreline $\zeta(t, 0)$ divided by $\tan^2(\alpha)$ for the initial pulse (a) and the incident pulse (b). The values for all parameters are the same as in figures 16 and 18.

Supplementary movies. Supplementary movies are available at https://doi.org/10.1017/jfm.2026.12121.

Acknowledgements. G.M. and M.H.M. would like to thank the Isaac Newton Institute for Mathematical Sciences, Cambridge, for support and hospitality during the programme 'Mathematical Theory and Applications of Multiple Wave Scattering' (January–June 2023), where this work was initiated, and during an INI retreat in December 2025, where the paper was finalised. These activities were also supported by the Simons Foundation. The authors thank the referees for their constructive comments, which improved the presentation of the manuscript.

Funding. The INI programme and retreat were supported by EPSRC grants EP/R014604/1 and EP/Z000580/1, respectively. G.M. acknowledges support from the EU H2020 MSCA RISE project EffectFact (grant no. 101008140) and a Royal Society Industry Fellowship. E.P. acknowledges support from the Russian Science Foundation (grant no. 22-17-00153) for the introduction and general discussions. M.H.M. acknowledges support from the Australian Research Council through Discovery Project DP240102104.

Declaration of interests. The authors report no conflict of interest.

Appendix A

In this section, we clarify the possible behaviour of the solution of the integral equation at zero and infinity using the governing functional equation (2.64). We start with rewriting the latter in the form

$$\tilde{p}_*^{(1)}(s+1) = \cot\frac{\pi s}{2}\big(\tan s(\theta_0-\pi))\tilde{p}_*^{(1)}(s) - \tilde{f}_{\clubsuit}^{(1)}(s)\big). \tag{A1}$$

Let us now take $s = -1+\delta$ ($\delta > 0$) and increase its value until the function $\tilde{p}_*^{(1)}(s+1)$ hits the first pole. If we assume that $0 < \alpha < \pi/4$, ($\pi < \theta_0 < 5\pi/4$), then the first pole of the right-hand side of the (A1) associated with the trigonometric function $\tan s(\theta_0 - \pi))$ involved (see also (2.52) and (2.64)) lies in the interval $2 < s < \infty$. Note that the points $s = 0, 1$ represent removable singularities. By direct computations, we obtain

$$\tilde{p}_*^{(1)}(1) = \frac{2\alpha}{\pi}\tilde{p}_*^{(1)}(0) - \left(1 - \frac{2\alpha}{\pi} + \frac{2\alpha}{\pi}d_1\right), \quad \tilde{p}_*^{(1)}(2) = -1 - d_1, \tag{A2}$$

https://doi.org/10.1017/jfm.2026.12121 Published online by Cambridge University Press

taking into account (2.83), those can be rewritten in the following manner:

$$\tilde{p}_*^{(1)}(0)\cos\nu = \frac{\pi}{2\alpha}\big(1+\tilde{p}_*^{(1)}(1)\big)\cos\nu - \cos\nu - \sin\nu, \tag{A3}$$

and

$$\tilde{p}_*^{(1)}(2)\cos\nu = -\cos\nu + \sin\nu. \tag{A4}$$

It is interesting to compare the above formula (A3) with that following from the knowledge of the run-up at the beach top (2.93). It suggests that $(1+\tilde{p}_*^{(1)}(1))\cos\nu = \sqrt{2\alpha/\pi}$.

Even though we computed the results in the figures 6(*a*), 9(*a*) and 11(*b*) by the latter, using (A3) provides more accurate way of computation due to the behaviour of the solution at infinity. Moreover, formula (A4) can serve as an additional check for computational accuracy. Here, we were provided by the preliminary knowledge of those parameters. In case of singular solution, similar identities will play a crucial role to detect missing information.

Finally, the next point on the run $s=2$ is a simple pole

$$\tilde{p}_*^{(1)}(s+1) \sim \frac{P_3^+}{s-2}, \quad s\to 2, \tag{A5}$$

where $P_3^+ = 4\pi^{-1}d_1 = -4\pi^{-1}\tan\nu$. This suggests that $\beta_\infty = 3$, at least, for $0<\alpha<\pi/4$.

Considering the remaining interval of the angle $\pi/4<\alpha\leqslant\pi$, we observe that there may appear another pole $s=\pi/(2\alpha)$ of the right-hand side of (A1) in the interval (0, 2) and the corresponding pole at point $s=1+\pi/(2\alpha)$ of the left-hand side

$$\tilde{p}_*^{(1)}(1+s) \sim \frac{P_*^+}{s-\pi/(2\alpha)}, \quad s\to\pi/(2\alpha), \tag{A6}$$

$$P_*^+ = -\frac{\cot(\pi^2/(4\alpha))\big(1+\tilde{p}_*^{(1)}(\pi/(2\alpha))\big)+d_1\big(1-1/\sin(\pi^2/(4\alpha))\big)}{\alpha},$$

thus in this case $\beta_\infty = 1+\pi/(2\alpha)$ for $\pi/4<\alpha\leqslant\pi$. It is clear from the analysis, that the next such pole appears when $s=1+3\pi/(2\alpha)$ and so on. In the limiting case, where $\alpha=\pi/4$ and solution $\tilde{p}_*^{(1)}(s)\equiv 0$, it is easy to observe that these two poles annihilate each other.

It is also important to observe that, in the case $\alpha=\pi/(2m)$, we have $s=\pi/2\alpha=m$ and the distribution of the poles looks identical to what we have described above while they annihilate each other as well. As a result, the function $\tilde{p}_*^{(1)}(s)$ is analytical in the entire half-plane.

To investigate possible poles of the function $\tilde{p}_*^{(j)}(s)$ with negative real part, we consider (2.64) rewritten conveniently in the form

$$\tilde{p}_*^{(j)}(s) = \cot s(\theta_0-\pi))\left(\tan\frac{\pi s}{2}\tilde{p}_*^{(j)}(s+1)+\tilde{f}_\clubsuit^{(j)}(s)\right). \tag{A7}$$

Utilising a similar analysis as above, we conclude that, for any $0<\alpha<\pi$, the closest negative pole of the right-hand side is $s=-1$ thus $\beta_0=1$ and

$$\tilde{p}_*^{(j)}(s) \sim \frac{P_{-1}}{s+1}, \quad s\to -1, \tag{A8}$$

$$P_{-1} = \frac{2\cot\alpha}{\pi}\left(\tilde{p}_*^{(j)}(0)+1+d_1\big(2\tan\alpha-1\big)\right). \tag{A9}$$

https://doi.org/10.1017/jfm.2026.12121 Published online by Cambridge University Press

Continuing the same procedure, we now consider points s within the interval $(-2, -1)$. For $0 < \alpha < \pi/2$, the next possible pole of the right-hand side may appear at the point $s = -2$ due to the simple pole of the function $\tilde{p}_*^{(j)}(s)$ at the point $s = -1$. However, the entire term $\tan(\pi s/2)\tilde{p}_*^{(j)}(s+1)$ has a finite limiting value as $s \to -2$, therefore, the function $\tilde{p}_*^{(j)}(s)$ is regular at the point $s = -2$). Its next negative pole represented by an entire number might be $s = -3$.

If we consider the remaining case, $\pi/2 < \alpha < \pi$, the next pole with the negative real part of the right-hand side in the functional equation (A7) may appear at the point $s = -\beta_1 = -\pi/\alpha < -1$ and

$$\tilde{p}_*^{(j)}(s) \sim \frac{P_*^-}{s + \pi/\alpha}, \quad s \to -\pi/\alpha, \tag{A10}$$

$$P_*^- = -\frac{1}{\alpha}\tan\frac{\pi^2}{2\alpha}\left(\tilde{p}_*^{(j)}(1-\pi/\alpha) + 1 + d_1\left(\cot\frac{\pi^2}{2\alpha} - \frac{1}{\sin\dfrac{\pi^2}{2\alpha}}\right)\right). \tag{A11}$$

Finally, we observe that in that limiting case, $\alpha = \pi$, there exists a double pole at the point $s = -1$ and

$$\tilde{p}_*^{(j)}(s) = \frac{Q_0 + (s+1)Q_1}{(s+1)^2} + O(1), \quad s \to -1, \tag{A12}$$

where

$$Q_0 = \frac{2\big(d_1 - \tilde{p}_*(0) - 1\big)}{\pi^2}, \quad Q_1 = \frac{\pi d_1 - 2\tilde{p}_*'(0)}{\pi^2}, \tag{A13}$$

where, for $\alpha = \pi$, d_1 can be computed from (2.83) and (2.91) to give $d_1 = \sqrt{2} - 1$.

References

Atkinson, C. 1977 On stress singularities and interfaces in linear elastic fracture mechanics. *Intl J. Fract.* **13**, 807–820.

Bennetts, L.G., Bitz, C.M., Feltham, D.L., Kohout, A.L. & Meylan, M.H. 2022 Theory, modelling and observations of marginal ice zone dynamics: multidisciplinary perspectives and outlooks. *Phil. Trans. R. Soc a* **380** (2235), 20210265.

Body, G.L. & Ehrenmark, U.T. 1998 Reflection of gravity waves by a steep beach with a porous bed. *J. Fluid Mech.* **359**, 265–280.

Brillouet, G. 1957 *Étude de quelques problèmes sur les ondes liquides de gravité*, vol. 329. En Vente au Service de Documentation et d'Information Technique de l.

Carrier, G.F. & Greenspan, H.P. 1958 Water waves of finite amplitude on a sloping beach. *J. Fluid Mech.* **4** (1), 97–109.

Chakrabarti, A., Mandal, B.N. & Gayen, R. 2005 The dock problem revisited. *Intl J. Math. Math. Sci.* **2005** (21), 3459–3470.

Dean, R.G. & Dalrymple, R.A. 1991 *Water Wave Mechanics for Engineers and Scientists*, vol. 2. World Scientific Publishing Company.

Didenkulova, I. 2009 New trends in the analytical theory of long sea wave runup. In *Applied Wave Mathematics* (ed. T.Q. Quak & E. Soomere), pp. 265–296. Springer.

Dobrokhotov, S.Y., Medvedev, B. & Minenkov, S. 2013 On transforms reducing one-dimensional systems of shallow-water to the wave equation with sound speed $c^2 = x$. *Math. Notes+*. **93**, 704–714.

Dorfman, A.A. 1984 Unsteady wave motions of a fluid above an inclined floor. *Fluid Dyn.* **19** (6), 914–918.

Ehrenmark, U.T. 1987 Far field asymptotics of the two-dimensional linearised sloping beach problem. *SIAM J. Appl. Math.* **47** (5), 965–981.

Ehrenmark, U.T. 1989 Overconvergence of the near-field expansion for linearized waves normally incident on a sloping beach. *SIAM J. Appl. Math.* **49** (3), 799–815.

https://doi.org/10.1017/jfm.2026.12121 Published online by Cambridge University Press

EHRENMARK, U.T. 1991 On viscous wave motion over a plane beach. *SIAM J. Appl. Math.* **51** (1), 1–19.
EHRENMARK, U. 1994 On computing uniformly valid approximations for viscous waves on a plane beach. *J. Comput. Appl. Math.* **50** (1), 263–281.
EHRENMARK, U.T. 2003 Wave trapping above a plane beach by partially or totally submerged obstacles. *J. Fluid Mech.* **486**, 261–285.
EHRENMARK, U. 2006 Application of the w-transformation to compute the linearised 2-d beach problem potentials. *J. Comput. Appl. Math.* **197** (2), 457–464.
EHRENMARK, U.T. 2009 On the normal incidence of linear waves over a plane incline partially covered by a rigid lid. *J. Fluid Mech.* **623**, 209–240.
EHRENMARK, U.T. 2011 A note on the computation of a green's function for short wavelength water waves over a plane incline. *J. Comput. Appl. Math.* **623**, 1667–1674.
EHRENMARK, U.T. & BODY, G.L. 2001 The initial-value problem on a plane beach. *Q. J. Mech. Appl. Math.* **54** (3), 389–411.
EHRENMARK, U.T. & PORTER, D. 2012 Water wave scattering by a floating elastic plate over a plane incline. *Q. J. Mech. Appl. Math.* **65** (3), 409–434.
FRIEDRICHS, K.O. 1948 Waves on a shallow sloping beach. *Commun. Pure Appl. Math.* **1** (2), 109–134.
FRIEDRICHS, K.O. & LEWY, H. 1948 The dock problem. *Commun. Pure Appl. Math.* **1** (2), 135–148.
GOKHBERG, I.T. & FELDMAN, I.A. 1974 *Convolution Equations and Projection Methods for Their Solution*. American Mathematical Society.
GRADSHTEYN, I.S. & RYZHIK, I.M. 2014 *Table of Integrals, Series, and Products*. Academic Press.
GRIFFEL, D.H. & MORRIS, C.A.N. 1977 An initial-value problem for waves over a sloping beach. *SIAM J. Appl. Math.* **33** (4), 535–541.
HAUGEN, K.B. & TYVAND, P.A. 2003 Radiation of water waves from an oscillating source located at a slope of angle $\pi/4$. *J. Engng Math.* **47**, 161–174.
ISAACSON, E. 1950 Water waves over a sloping bottom. *Commun. Pure Appl. Math.* **3** (1), 11–31.
KELDYSH, M.V. 1937 The problem of the reflection of waves on the surface of a heavy fluid. In *Third Conference on Wave Resistance Theory [in Russian]*. pp. 140–142. Izd. TsAGI.
KOITER, W.T. 1955 On the diffusion of load from a stiffener into a sheet. *Q. J. Mech. Appl. Math.* **8** (2), 164–178.
KUZNETSOV, N.G., MAZ'YA, V.G. & VAINBERG, B. 2002 *Linear Water Waves: A Mathematical Approach*. Cambridge University Press.
KÂNOĞLU, U. & SYNOLAKIS, C. 2006 Initial value problem solution of nonlinear shallow water-wave equations. *Phys. Rev. Lett.* **97** (14), 148501.
LAWRIE, J.B. & KING, A.C. 1994 Exact solution to a class of functional difference equations with application to a moving contact line flow. *Eur. J. Appl. Math.* **5** (2), 141–157.
LEWY, H. 1946 Water waves on sloping beaches. *Bull. Am. Math. Soc* **52**, 737–775.
MALIUZHINETS, G.D. 1958 Excitation, reflection and emission of surface waves from a wedge with given face impedances. *Soviet Phys. Dokl.* **623**, 752–755.
MEI, C.C. 1989 *The Applied Dynamics of Ocean Surface Waves*, vol. 1. World Scientific.
MEYLAN, M.H. 2009 Time-dependent linear water-wave scattering in two dimensions by a generalized eigenfunction expansion. *J. Fluid Mech.* **632**, 447–455.
MICHE, A. 1944 Mouvements ondulatoires de la mer en profondeur constante ou décroissante. *Ann. Ponts Chaussees* **25**, 369–406.
MISHURIS, G.S. 1995*a* Bound*a*ry value problems for poisson's equation in a multi-wedge – multi-layered region. *Arch. Mech.* **47** (2), 295–335.
MISHURIS, G.S. 1995*b* On a class of singular integral equations. *Demonstr. Math.* **28** (4), 781–794.
MISHURIS, G. 2001 Interface crack and nonideal interface concept (Mode III). *Intl J. Fract.* **107**, 279–296.
PELINOVSKY, E.N. & MAZOVA, R.K. 1992 Exact analytical solutions of nonlinear problems of tsunami wave run-up on slopes with different profiles. *Nat. Hazards* **6**, 227–249.
PETERS, A.S. 1950 The effect of a floating mat on water waves. *Commun. Pure Appl. Math.* **3** (4), 319–354.
RODRIGUEZ-DELGADO, C., BERGILLOS, R.J. & IGLESIAS, G. 2019 Dual wave farms for energy production and coastal protection under sea level rise. *J. Clean. Prod.* **222**, 364–372.
RUMYANTSEV, B.N. 1960 Unsteady motions of a heavy fluid on an inclined shore. *Prikl. Mat. Mekh* **24** (3), 540–544.
RYBKIN, A. 2019 Method for solving hyperbolic systems with initial data on non-characteristic manifolds with applications to the shallow water wave equations. *Appl. Math. Lett.* **93**, 72–78.
SHINBROT, A.F.M. 1967 The initial value problem for the linearized equations of water waves. *J. Math. Mech.* **17** (2), 107–180.

https://doi.org/10.1017/jfm.2026.12121 Published online by Cambridge University Press

SINGHVI, A., LUIJENDIJK, A.P. & VAN OUDENHOVEN, A.P.E. 2022 The grey–green spectrum: a review of coastal protection interventions. *J. Environ. Manage.* **311**, 114824.
SPIELVOGEL, L.Q. 1976 Single-wave run-up on sloping beaches. *J. Fluid Mech.* **74** (4), 685–694.
SRETENSKY, L.N. 1977 *Theory of Wave Motions in Fluids (in Russian)*, p. 816. Nauka.
STOKER, J.J. 1947 Surface waves in water of variable depth. *Q. Appl. Math.* **5** (1), 1–54.
STOKER, J.J. 2019 *Water Waves: The Mathematical Theory with Applications*. Courier Dover Publications.
SYNOLAKIS, C.E. 1987 The runup of solitary waves. *J. Fluid Mech.* **185**, 523–545.
TEMAM, R. 2024 *Navier–Stokes Equations: Theory and Numerical Analysis*, vol. 343. American Mathematical Society.
TON, B.A. 1987 Water waves over a sloping beach. *J. Math. Anal. Appl.* **122** (2), 555–581.
WANG, C.D. & MEYLAN, M.H. 2002 The linear wave response of a floating thin plate on water of variable depth. *Appl. Ocean Res.* **24** (3), 163–174.
WikiWaves 2010 Boundary element method for a fixed body in finite depth. Available at: https://wikiwaves.org/index.php/Boundary_Element_Method_for_a_Fixed_Body_in_Finite_Depth. [Online; accessed 15 June 2025].
WILKS, B., MEYLAN, M.H., MONTIEL, F. & WAKES, S. 2024 Generalized eigenfunction expansion and singularity expansion methods for two-dimensional acoustic time-domain wave scattering problems. *Proc. R. Soc. A* **480** (2297), 20230845.
WILKS, B., MEYLAN, M.H., MONTIEL, F. & WAKES, S. 2025 Generalised eigenfunction expansion and singularity expansion methods for canonical time-domain wave scattering problems. *Wave Motion* **132**, 103421.
ZEMANIAN, A.H. 1987 *Distribution Theory and Transform Analysis: an Introduction to Generalized Functions, with Applications*. Courier Corporation.

https://doi.org/10.1017/jfm.2026.12121 Published online by Cambridge University Press